Review article

Xuewen Wang*, Zhongquan Nie, Yao Liang, Jian Wang, Tao Li and Baohua Jia*

Recent advances on optical vortex generation

https://doi.org/10.1515/nanoph-2018-0072
Received June 13, 2018; revised July 25, 2018; accepted July 27, 2018

Abstract: This article reviews recent progress leading to the generation of optical vortex beams. After introducing the basics of optical vortex beams and their promising applications, we summarized different approaches for optical vortex generation by discrete components and laser cavities. We place particular emphasis on the recent development of vortex generation by the planar phase plates, which are able to engineer a spiral phasefront via dynamic or geometric phase in nanoscale, and highlight the independent operation of these two different phases which leads to a multifunctional optical vortex beam generation and independent spin-orbit interaction. We also introduced the recent progress on vortex lasing, including vortex beam generation from the output of bulk lasers by modification of conventional laser cavities with phase elements and from integrated on-chip microlasers. Similar approaches are also applied to generate fractional vortex beams carrying fractional topological charge. The advanced technology and approaches on design and nanofabrications enable multiple vortex beams generation from a single device via multiplexing, multicasting, and vortex array, open up opportunities for applications on data processing, information encoding/decoding, communication and parallel data processing, and micromanipulations.

Keywords: optical vortex; orbital angular momentum; dynamic phase; geometric phase; metasurfaces; spin-orbit interaction; vortex lasers; fractional vortex; multiplexing; multicasting; vortex array generation.

1 Introduction

Optical vortex refers to a beam of photons that propagates with a singularity in phase taking the form of $e^{i\ell\varphi}$ about its axis (φ is the azimuthal coordinate in the transverse plane and ℓ is an integer quantum number) and has a topological structure on its wavefront with topological charge ℓ arising from its helicoidal spatial wavefront around the phase singularity. The topological structure in the wavefront is not only limited to light, but can also be found in other forms, such as acoustic wave [1], electrons [2, 3], and neutrons [4]. At the singularity, the phase is undeterminable and the polarization and amplitude vanish altogether, resulting in a dark centre within the wavepacket. This singularity was first introduced as a screw dislocation in wave trains similar to the crystal dislocations [1]. Such dislocations in light wavefront were later found to be a universal phenomenon. They were not only observed in the special laser beams but also were predicted and observed in the laser scattering speckle field, in which the dark speckle has an optical vortex, resulting from the interfering of multiple plane waves [5–9]. Optical vortices in the scattering field were found to behave similarly like charged particles in some instances [1]. During the propagation, they may rotate around the axis or interact with the surrounding optical vortices, repelling or attracting each other or even annihilating in collision, or generating other type of wavefront defects [10–13]. An isolated optical vortex preserves its topological charge and robust to perturbations in propagation even through the atmospheric turbulence [10, 12–16]. These features in the phase singularity attracted more interests when they were linked to the angular momentum of the beam in 1992 [17]. An optical vortex beam possessing a phase singularity with a spiral wavefront was found carrying quantized orbital

***Corresponding authors: Xuewen Wang and Baohua Jia,** Centre for Micro-Photonics, Faculty of Science, Engineering and Technology, Swinburne University of Technology, Hawthorn, VIC 3122, Australia, e-mail: xuewenwang@swin.edu.au (X. Wang); bjia@swin.edu.au (B. Jia). http://orcid.org/0000-0003-3751-0306 (X. Wang)
Zhongquan Nie: Centre for Micro-Photonics, Faculty of Science, Engineering and Technology, Swinburne University of Technology, Hawthorn, VIC 3122, Australia; and Key Laboratory of Advanced Transducers and Intelligent Control System, Ministry of Education and Shanxi Province, College of Physics and Optoelectronics, Taiyuan University of Technology, Taiyuan 030024, China
Yao Liang: Centre for Micro-Photonics, Faculty of Science, Engineering and Technology, Swinburne University of Technology, Hawthorn, VIC 3122, Australia
Jian Wang: Wuhan National Laboratory for Optoelectronics, School of Optical and Electronic Information, Huazhong University of Science and Technology, Wuhan 430074, Hubei, China
Tao Li: National Laboratory of Solid State Microstructures, College of Engineering and Applied Sciences, School of Physics, Nanjing University, Nanjing, China

angular momentum (OAM), with $\ell\hbar$ per photon, which can be many times larger than the spin angular momentum (SAM)($\pm\hbar$ per photon) associated with the photon spin [17]. Generating a vortex laser beam using large Fresnel number of the cavity was found to be possible and was implemented by transforming the high-order Hermit-Gaussian (HG) modes into Laguerre-Gaussian (LG) beam with a pair of cylindrical lenses [17, 18]. Since then, intensive investigations and efforts have been focused on optical vortices and their propagation properties with conserved topological charge and angular momentum in linear and nonlinear media [13–15, 19–23].

A significant work is the direct observation of the transfer of OAM of light to matter, resulting in the spinning of the micro object [24]. This opens a new direction for micromanipulation using optical tweezers [23–30]. Besides the ability to transfer angular momentum to the object, the topologically protected and state unbounded properties of OAMs provide a potential to encode information in a new infinite freedom. This leads to a possible solution to the current massive data challenge and has the chance to dramatically boost the capacity of optical communication and data storage [31–35]. These properties not merely attract the interests from researchers in the classical optical communication fields, but also are appealing to those working in the quantum information and technology domains. Discrete higher dimensional quantum systems, also called as qudits, were demonstrated to be formed by the OAM states of photon [36]. Each qudit will not be limited to two states, but theoretically can have any number of discrete levels. Hence, each single photon in the optical vortices can be used to encode information more than one bit, which offers great potential for quantum technologies [36–39]. Other promising diverse applications were also proposed and developed in the recent years, such as microscopy imaging [40–42], material processing [43–45], metrology [46–48], and astronomy [49–51].

All of these potential promising applications drive the demand on producing versatile and diverse optical vortex beams. The further demand of miniaturizing the feature dimensions of optical components as well as developing highly integrated optical devices requires new concepts and approaches to achieve this. Sophisticated and advanced nanofabrication techniques are presenting golden opportunities to manipulate the energy flow of light in micro-/nanoscale, which leads to a new plateau of vortex generation [52–55].

Our aim in writing this review has been to strive to provide a current state of the optical vortex beam generation to improve the compactness and functionality. There are few reviews focused on the general introduction about the development of OAMs of light [25, 56, 57]. For a general introduction on OAMs and their applications, the readers can refer to the previous review [29]. For more focused applications of OAMs, interested readers can refer to the recent published review papers on micromanipulation [27], optical communication [58, 59], and quantum technology [60]. In this review, a general introduction about optical vortex and their emerging applications is presented in Section 1 and an overview of the development on generating optical vortex beams will be presented in Section 2. The advanced techniques on optical vortex beam generation with discrete planar elements that introduce a dynamic helicoidal phase, geometric phase, or hybrid phase are introduced in Section 3. Advances of optical vortex beam generated directly from laser sources in the bulk or on chip are summarized in Section 4. Section 5 brings the approaches on generation of optical vortices carrying non-integer OAMs. And in Section 6, state-of-the-art techniques on simultaneously generating multiple vortex beams from a single device are introduced, including OAM multiplexing that generates multiple optical vortex beams from multiple Gaussian beams and vice versa, OAM multicasting that generates multiple coaxial optical vortex beams from single input Gaussian beam, and optical vortex arrays that generates spatially distributed optical vortex beams. Finally, we conclude in Section 7.

2 Overview

After significant work of the optical vortex beam generation in 1992 [19], various approaches were developed in succession. The early endeavours were focused on modifying the Gouy phase shift of the beam, using a pair of cylindrical lenses as mode converters to transform HG modes to LG modes. In principle, any HG modes aligning at $\pi/4$ with respect to the axis of the lens can be converted into LG modes with the same beam waist. A generalized description of the transformation between the arbitrary order of HG modes and LG modes and vice versa using mode converters were presented [19]. By inserting opaque wires or shifting the geometric alignment to off-axis from the cavity, different high order of HG modes can be excited; then assisting with the mode converters, high order of LG laser beams carrying large number of OAMs can be created [61–63].

The most direct way to create a helical wavefront is to allow the light beam to propagate into a medium with

spiral inhomogeneity in the longitudinal direction to generate an integer phase step along the azimuthal angle. A simple way is to fabricate a plate with a helical surface called as spiral phase plate (SPP), which was first implemented in 1994 [20]. To facilitate the fabrication process, normally the helical surface will be discretized into different steps as diffractive elements. By matching the refractive index, the working wavelength can be slightly tuned. Another method is based on computer-generated hologram (CGH) to generate optical vortices. An optical vortex beam carrying a spiral wavefront collinearly interfered with a Gaussian beam creates a spiral interfering fringe, in which the number and the rotating direction of the spiraling arms indicate the number and sign of the topological charge respectively. When it interferes with an off-axis plane wave, a fork grating is created with a clear defect on fringes where a phase singularity locates. These unique interference patterns were also widely used to characterize the topological charge of a vortex beam. Based on the property of the interference, a hologram plate can be generated from the spiral fringe or the fork grating [64]. This approach is widely used with commercial spatial light modulators (SLMs) based on pixelated liquid crystals, which can be programed to generate holograms via a convenient user interface.

The above-proposed approaches to generate optical vortex did not take into consideration of the possible interaction between the SAM and OAM of the beam (both intrinsic and external OAM) [22]. Namely, the generated OAMs are polarization independent, and the wavefront is modified by the propagation accumulated phase, which is also called dynamic phase. In 2002, engineering the wavefront to produce a helical phase using artificially anisotropic inhomogeneous medium was proposed based on subwavelength gratings [65]. This approach manipulates the polarization state of the emerging beam using spatially distributed polarization converters to introduce a geometric phase, which is also called Pancharatnam-Berry phase, as a counterpart of the dynamic phase. Patterning the birefringence media such as subwavelength gratings and liquid crystals gives rise to the conversion between SAM and OAM [65, 66]. The value of OAMs that each photon carries is determined by the number of rotations of the optical fast or slow axis along the azimuthal angle. The spin to orbital angular momentum conversion attributed from the geometric phase provides a totally different approach to generate the optical vortex via polarization manipulation rather than propagation path engineering. In this context, the generation of vector vortex beams is enabled by synchronously tailoring the polarization and phase patterns of the wavefront related to spin-orbital angular momentum coupling [67–69]. Altering the dynamic phase and geometric phase could be an independent process. It offers an opportunity to manipulate the wavefront embedding both the dynamic and geometric phase simultaneously, thus leading to the creation of complexed and multifunctional light beams. In addition, yet another exotic OAM mode coined as perfect vortex beam, whose dark hollow area is immune to the topological charge, is able to be acquired based on geometric phase element [70, 71], Fourier transform optical system [72, 73], or tightly focused configuration [74].

Generating optical vortex beams via discrete components with bulky or planar elements encounters a low signal-noise ratio (SNR) due to its low purity of spatial modes, which is critical and inevitable in many applications. Optical vortex lasers are optical coherent sources directly emitting light beams carrying certain amount of OAMs. The OAM modes generated from a vortex laser has extreme high purity because of the desired polarization and spatial mode being amplified in the gain medium after each cycle. As for the undesired polarization or mode distributions, they simply fail to form a stable resonance in the cavity and end up vanishing in the laser mode competition. Active vortex lasing creating OAM-carrying modes directly in cavities is challenging from OAM modes degeneracy and OAM handedness selection [75–77].

In addition to the aforesaid integer-order OAM beams, vortices with fractional topological charge have gain ever more compelling interests over the past decade. Distinguished from a vortex beam with integer topological charge with reference to the intensity pattern, the fractional-order OAM beams possess a unique line of low intensity due to the phase step on π along the null azimuthal angle orientation. It has been demonstrated that upon propagation such beams exhibit a rich phase evolution consisting of a chain of alternating vortices near the radial dislocation [78]. These peculiar light fields rapidly emerge as viable tools for particle manipulation and quantum communication, and simultaneously offer a new insight into the singular optics.

Control over the versatile generation approaches of the vortex beams carrying OAMs has been advanced at an unrivalled pace in the last couple of decades. Equally impressive are their possible potential avenues of applications ranging from micromanipulation, optical microscopy, secure computation to classical and quantum communications, among other feats. From a more practical front, it is vigorously desired for the generation of multiple OAM beams with the features of being flexibly tunable to fulfil the urgent requirements of current multiplexing technology. Diverse schemes have been so far put forward

for the parallel processing of OAM beams, including OAM multiplexing, OAM multicasting, and optical vortex array generation via a single device.

3 Planar optical vortex generator

3.1 Dynamic phase plate

The generation of optical vortex beam upon accumulated propagation effect relies on physical propagation distance, passing through a media with given refractive index. An SPP is such an element with a gradient of thickness varying along azimuthal angle according to $\partial h/\partial\varphi = \ell\lambda/2\pi(n-1)$, where n is the refractive index of the material and λ is the free-space wavelength of the beam. When light passes through an SPP, a helicoidal phase is imposed into the wavefront. To minimize the distortion of the wavefront and precisely produce the desired topological charge for certain wavelength, the surface quality of SPP needs to be well controlled. Conventionally, SPPs are fabricated in the same way as other diffractive optics. When higher number of topological charge is desired, multiple steps of lithography and higher angular resolution are required. Along with the development as other nanofabrication techniques, femtosecond laser direct writing has been demonstrated as an effective micro- and nanofabrication tool [79–83]. Energy of photons can be precisely controlled and delivered into the spatially confined volume via multi-photon absorption with tightly focused femtosecond laser pulses. The resolution of femtosecond laser direct writing has reached to smaller than 100 nm [84, 85]. An SPP with continuous thickness gradient to generate optical vortex with topological charge $\ell = 1$ was demonstrated [86], which has a controlled surface accuracy better than $\lambda/15$, as shown in Figure 1A. This unrestricted 3D structuring technique provides the possibility to fabricate SPPs integrating with other optical components with high surface quality, such as SPPs fabricated on the tip of optical fibres to precisely generate optical vortex beams with different topological charges [89].

Comparing to the micro-SPPs fabricated by 3D femtosecond laser direct writing, there is another approach which is able to further downscale the size of the device to generate polarization independent optical vortex beams. By introducing a phase discontinuity along

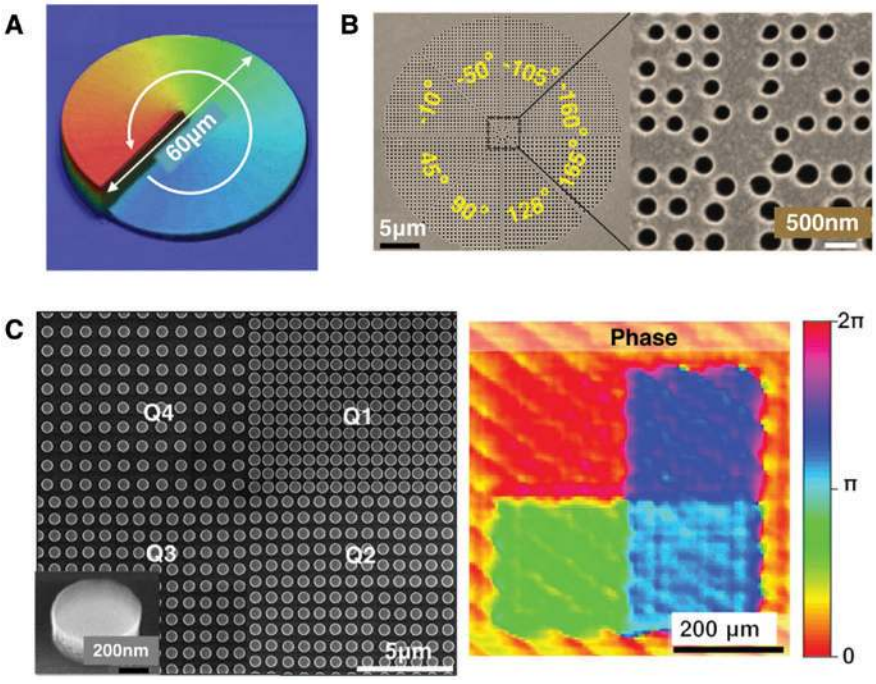

Figure 1: Optical vortex beam generated by dynamic phase plates.
(A) Optical profilometry image of a 60-μm diameter 3D femtosecond laser printed mirco-SPP with continuous phase changing generates optical vortex with topological charge $\ell = 5$ at 633 nm. Reprinted from Ref. [86]. (B) Nanowaveguide array with a phase modulation covers 2π full range, generating optical vortex with topological charge $\ell = 1$ at 532 nm. Reprinted from Ref. [87]. (C) Silicon nanodisks with high refractive index. Reprinted from Ref. [88].

the interface using ultrathin subwavelength nanostructures, which are also called metasurfaces, it is possible to control the reflection and refraction according to the generalized Snell's law [90]

$$\begin{cases} \sin(\theta_t)n_t - \sin(\theta_i)n_i = \lambda\nabla\Phi/2\pi \\ \sin(\theta_r) - \sin(\theta_i) = n_i^{-1}\lambda\nabla\Phi/2\pi \end{cases} \quad (1)$$

where θ_t, θ_i, θ_r are the angles of refraction, incidence, and reflection, respectively; n_t and n_i are the refractive index of the media in the transmission and incidence side, respectively; and $\nabla\Phi$ is the gradient of phase discontinuity along the interface. This phase discontinuity can be achieved by utilizing subwavelength metallic nanoantennas, scatters, or thin films [90–94]. By exciting the localized plasmonic resonance of the resonators with different geometry, the scattering field can lead or lag the excitation field, resulting to the tuning of the phase discontinuity. This tuning is limited into 0 to π range for a single nanoantenna, arising from the nondirectionally scattered electric field by the nanoantenna [94–96]. This can be overcome by using multiple-layered metasurfaces, or scatters with multiple independent resonances or coupled antenna resonances, which are able to extend the phase tuning to the entire 2π range without altering polarization [87, 96–98]. Comparing to the conventional phase accumulation effect, this abrupt phase can be introduced by the resonators with negligible thickness. By spatially engineering the gradient of phase discontinuity along the azimuthal angle on the interface, optical vortex beams carrying helical phasefront can be generated by the ultra-compact and ultrathin devices. In Figure 1B, an array of nanowaveguides was designed to introduce a phase change determined by the geometry of the waveguides [87]. These waveguides are composed of circular nanoholes milled in a thin silver film and filled with dielectric material. By changing the radius of the nanoholes, the resonated scattering field and the waveguide modes will be excited and lead to a phase tuning be able to cover 2π range. The symmetric geometric ensures the insensitivity to the exciting polarization field. Arranging the distribution of nanowaveguides according to $\Phi(r) = \ell\phi$ (r is the radius of the nanowaveguide), an optical vortex beam which carries OAM is converted from Gaussian beam by an ultrathin metallic metasurface. The transmitted power of the converted optical vortex beam from such thin device is very low, due to the prominent Ohmic loss and absorption in the optical frequency. Furthermore, the mismatch with the free-space impedance leads to backreflection of the incident power and reduces the conversion efficiency [97–99]. Another solution is to use thicker high refractive index dielectric materials to replace metals [100–103]. The strong localized electric and magnetic resonances of dielectric particles have been observed and enable a phase coverage of 2π without changing polarization in a single thin layer [104–106]. Therefore, comparing to a single metallic particle, a high refractive index dielectric particle provides the opportunity to tune both electric and magnetic resonances, as well as their interactions with nearby scatters. This provides an opportunity for full wavefront control with identical nanoparticles and simplifies the design and fabrication process. Figure 1C shows a dielectric metasurface vortex generator consisting of cylindrical silicon nanodisks, which enables a transmission efficiency more than 70% [88]. By varying the lattice constant in the disk arrays, the coupling strength between the adjacent disks can be controlled, leading to a full tuning of the phase.

The capability to modulate both phase and amplitude of light using metasurfaces has enabled ultrathin and high resolution computer-generated holographic technique to store and recover information [107–109]. Comparing to the conventional CGHs, metasurface holograms can encode information into a negligible thickness with high efficiency [107, 109]. Interference fringes of a vortex beam with Gaussian beams or plane wave carries its phase information, which was widely used to produce optical vortex beams. A meta-fork grating plate with an open aperture was reported to produce optical vortices being able to carry arbitrary rational OAMs [110], as shown in Figure 2A. A phase profile possessing regular singularities was encoded into the fork-grating, it continuously generates different optical vortex beams at different size of aperture when a plane wave passing through it. Spiral fringes formed by a vortex beam coaxially interfering with a Gaussian beam also can be encoded into a metasurface hologram to generate vortex beams. A spiralling-fringe hologram composed by low refractive index silicon nitride ($n \approx 2$) nanorod arrays with thickness $t = \lambda$ and period $p = 0.7\lambda$, was designed to generate optical vortex beam with topological charge $\ell = 1$ at wavelength $\lambda = 633$ nm [111], as shown in Figure 2B. By changing the duty cycle, a full coverage of 2π was achieved. A spiral phasefront was recovered from this hologram when a Gaussian beam was illuminated. The function of a CGH was further explored to shape the propagation of light based on metasurfaces. It can be designed to be dispersionless or wavelength-/polarization-multiplexing encoded [113–115]. A metasurface hologram composed of polarization sensitive metallic nanoslits was designed to generate optical vortex and airy beam at different polarization states from a single element [112]. The schematics of the design procedure of the metasurface hologram and the generation of optical

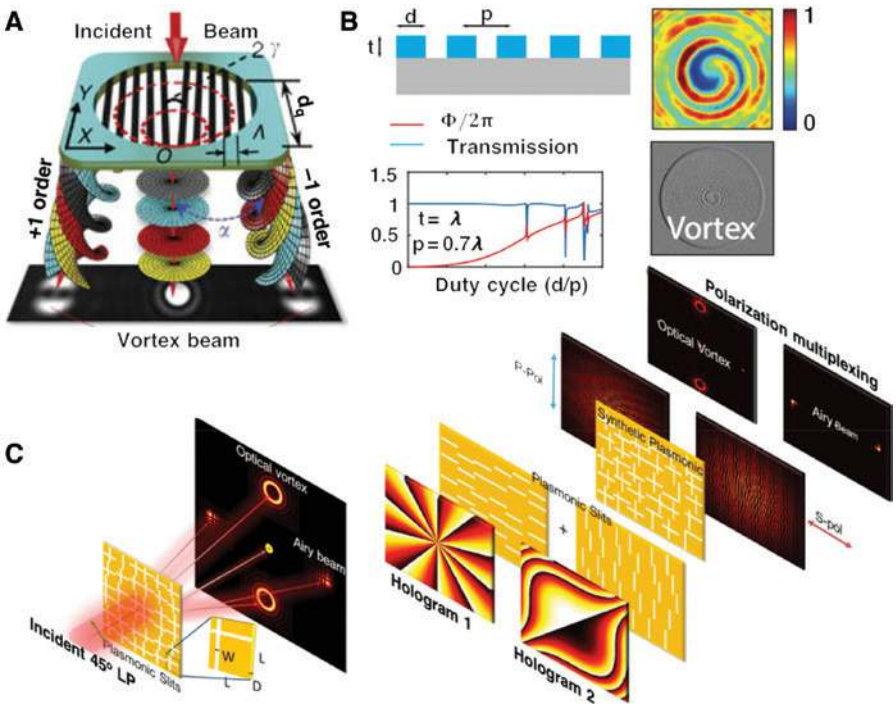

Figure 2: Optical vortex beam generated by metasurface holograms.
(A) Sketch of the metasurface fork grating hologram with an open circular aperture generates different optical vortices depending on the size of the aperture. Reprinted from Ref. [110]. (B) A spiral metasurface hologram composed of silicon nitride nanorods generates an optical vortex with topological charge $\ell = 1$. A full phase control implemented by tuning the coupling strength of adjacent scatters via tuning the duty cycle. Reprinted from Ref. [111]. (C) Schematic of the design of a multifunctional metasurface hologram based on orthogonal nanoslits that generates optical vortices and Airy beams simultaneously. Reprinted from Ref. [112].

vortices and airy beam from it are shown in Figure 2C. By adjusting the distance of adjacent slits, full modulation of the wavefront was achieved via a polarization control.

3.2 Geometric phase plate

When a polarized beam undergoes a closed loop on the Poincaré sphere, it acquires not only a dynamic phase, but also a geometric phase, which is half of the solid angle in the closed loop on the Poincaré sphere, firstly proposed by Pancharatnam [116]. It was further developed by Berry in 1987, via connecting to the adiabatic phase change of a slow cyclic quantum system, and regarded as an optical analogue to the Aharonov-Bohm effect [116–118]. This geometric phase arising from polarization manipulation was also called Pancharatnam-Berry phase. The phase velocity of two linearly orthogonal polarized components are different when light is propagating in an anisotropic material. The natural anisotropic material normally refers to crystals with different optical axes. By applying external fields on any isotropic material that temporally or permanently break the symmetry of the dielectric tensors along the propagation direction, for example, applying electric or magnetic fields, or mechanical stress field, artificial optical anisotropic materials can be created [119–122]. Another approach is to employ subwavelength structures with polarization sensitive response to create artificially desired anisotropy [123–126]. By varying the orientation of the optical axis of the birefringence in a rotationally symmetric geometry, the SAM of light will convert into its OAM. The wavefront of the emerging beam carries optical vortices. It is convenient to use the Jones matrix to describe the space-variant birefringence plate, and can be written

$$T = R(\theta)^{-1}\begin{bmatrix} t_x & 0 \\ 0 & t_y e^{i\delta} \end{bmatrix} R(\theta) \tag{2}$$

where $R(\theta)$ is the rotation matrix, $\theta(x, y)$ orientation of the optical axis, t_x and t_y the transmission amplitude of TE and TM components, and δ the phase retardation. For any input polarization $|E_{in}\rangle$, the output after passing the element can be decomposed into three components in helical basis [127, 128]

$$|E_{out}\rangle = \sqrt{\eta_E}\,|E_{in}\rangle + \sqrt{\eta_R}\,e^{i2\theta}\,|R\rangle + \sqrt{\eta_L}\,e^{-i2\theta}\,|L\rangle \tag{3}$$

where $|R\rangle$ and $|L\rangle$ are right-hand or left-hand circular polarization, $\eta_E = \left|\frac{1}{2}(t_x + t_y e^{i\delta})\right|^2$, $\eta_R = \left|\frac{1}{2}(t_x - t_y e^{i\delta})\langle L|E_{in}\rangle\right|^2$, and $\eta_L = \left|\frac{1}{2}(t_x - t_y e^{i\delta})\langle R|E_{in}\rangle\right|^2$ are the coefficients of each component, respectively. The first component keeps the same polarization state as incident, and the second or third component undergoes a SAM conversion associating with a geometric phase $\Phi_{PB} = 2\sigma\theta$. Neglecting the absorption and loss of the element, for a pure circularly polarized incident beam, the conversion efficiency reaches 100% when the retardation is $\delta = \pi$, working as a half-wave plate. The right-hand circular polarization was totally converted to left-hand circular polarization via different loops on the Poincaré sphere, and vise versa. Hence, by patterning the anisotropy, ultra-thin spin-dependent optical elements with desirable phase modulation can be achieved [127–129].

At a rotationally symmetric geometry, $\theta(x, y) = q\phi$ (q is the constant angular rotation velocity of the anisotropy), the emerging beam carries a spiral phasefront of $\Phi_{PB} = 2q\sigma\phi$, with a topological charge $\ell = 2q\sigma$, which was also interpreted as the result of spin-orbit interaction [65, 130–135]. In 2002, a vortex beam was generated via a spatially-variant subwavelength dielectric gratings in the mid-infrared limited by the fabrication resolution [65], and similar thin elements were further demonstrated in the visible range recently [128]. Patterned liquid crystals naturally possessing anisotropy were also reported to generate optical vortex [66]. Geometric phase metasurfaces composed of identical subwavelength nanoantennas with a phase retardation close to π were widely used to engineer the wavefront [127–131, 136–138]. A geometric phase metasurface with space-variant nanoslits on thin gold film was reported to be able to generate high purity optical vortices with topological charge up to $|\ell| = 10$ in the visible range [139]. A single slit with width 160 nm, thickness 300 nm, and period 500 nm results to a retardation of π. The nanoslits were patterned along the azimuthal angle with $\theta = 5\phi$. For the circularly polarized incident beam $\sigma_{in} = \pm 1$, the optical vortex possesses an opposite handedness and a topological charge $\ell = \mp 10$, respectively. The metallic geometric phase plate and the intensity profile of the generated optical vortex and their spiral interference patterns from different circularly polarized incident beams were shown in Figure 3A. Such metallic geometric phase plates suffer the same problems as mentioned before. Dielectric scatters with high transmission and low loss have been reported to efficiently generate optical vortex beams [142].

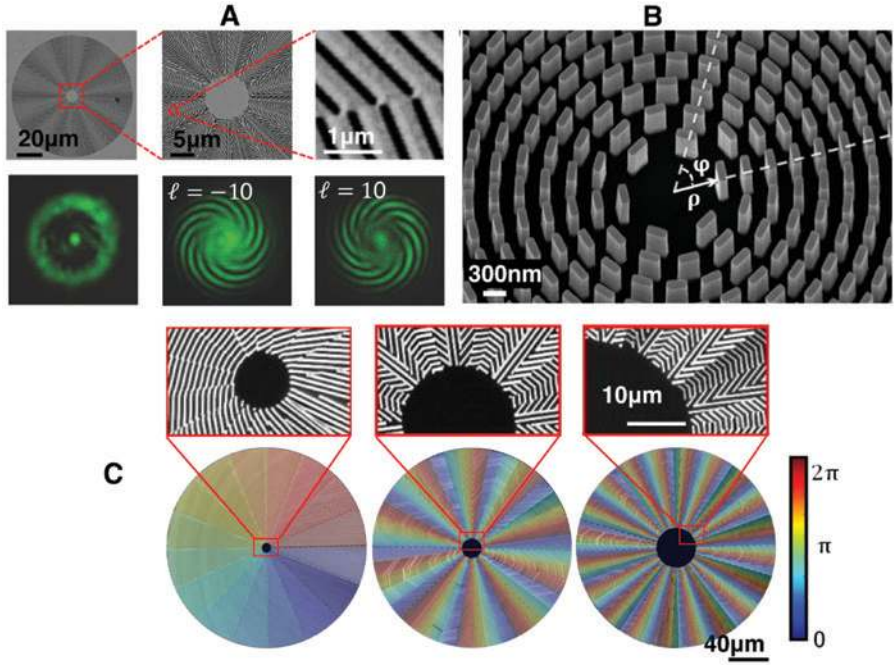

Figure 3: Optical vortex beam generated by geometric phase metasurfaces.
(A) A geometric phase metasurface based on gold nanoslits generates optical vortex beams with topological charge $\ell = \pm 10$, when incident is left-hand or right-hand circularly polarized, respectively. Reprinted from Ref. [139]. (B) A dielectric metasurface composed of TiO_2 nanofins with orientation varying from 0 to 2π induces a geometric phase from 0 to 4π along the azimuthal direction. Reprinted from Ref. [140].
(C) Geometric phase plates generates high orders of optical vortex beams fabricated by femtosecond laser printing. Reprinted from Ref. [141].

To further increase the conversion efficiency for the visible wavelength, titanium dioxide (TiO_2) nanofins were used [140]. Figure 3B shows a dielectric geometric phase plate with identical TiO_2 nanofins with 90 nm wide, 250 nm long and 600 nm tall, with changing orientation $\theta=\phi$, which is able to generate a vortex beam with topological charge $|\ell|=2$, with a reported efficiency around 60% at 532 nm. A further lower refractive index material with photoresist was used to enable the spin-orbit interaction [141]. A retardation of π is possible to be achieved based on the subwavelength gratings patterned on photoresist by femtosecond laser direct writing. This technique is scalable and allows integration with other optical components. Three phase plates were shown in Figure 3C, which are able to generate optical vortex with topological charge $|\ell|=1, 10, 20$, respectively. The colours on the element indicate the geometric phase modulation arising from its anisotropy variation.

3.3 Hybrid phase plate

3.3.1 Phase compensation for full wavefront control

The independent behaviour of engineering dynamic and geometric phase provides more freedom for phase modulation using nanostructures. The broadband nature of geometric phase was used to compensate the dispersion of the coupling resonances of metallic and dielectric nanostructures, enabling the operation of the device in a broad spectral range [143–146]. A single or localized resonance is not sufficient for modifying the phase within a full coverage. Except tunning multiple resonances or the coupling strength between adjacent scatters, modifying the polarization to introduce a Pancharatnam-Berry phase was adopted into designing hybrid metasurfaces for full wavefront control. Figure 4A shows a metallic V-shaped nanoantenna producing a controllable phase modulation over the π-phase range with designed geometry [90]. By rotating $\pi/2$ of each element, a geometric phase containing π was obtained, thus leading to a complete modulation of the wavefront. The polarization conversion efficiency in this case is very low, considering the retardation $\delta\neq\pi$ for the whole set of antennas and low scattering efficiency. A set of silicon nanofins were designed to keep a retardation $\delta\approx\pi$ in a very broad spectral range, and with near unit reflection efficiency [142], as shown in Figure 4B. After rotating $\pi/2$ of each nanofin, an additional phase was achieved. Azimuthally pattering the antennas into different discretised sectors, an optical vortex plate was designed.

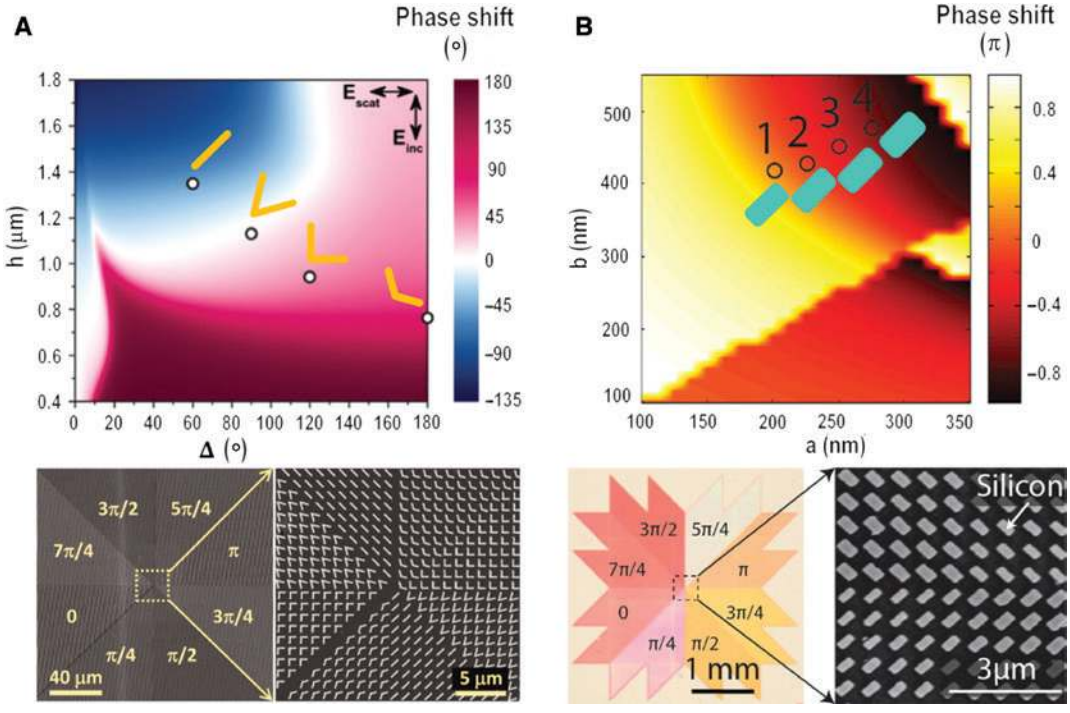

Figure 4: Geometric phase enables a full phase control of nanoattenas to generate optical vortex.
(A) Phase ramp of a set of four V-shaped nanoattenas covers from 0 to π, by rotating the element with $\pi/2$, additional phase with π arising from the geometric phase enables the optical vortex generation after pattering along the azimuthal direction. Reprinted from Ref. [90]. (B) A hybrid dielectric metasurface composed of silicon nanorods enables high conversion efficiency in a broad spectral range. Reprinted from Ref. [142].

3.3.2 Multifunctional spin-dependent optical vortex beam generation

In some of the applications, the intrinsic high divergence of a vortex beam during propagation may not be preferred. Instead of introducing a bulky element to focus the beam, an ultrathin element directly generates a focusing vortex beam is desired. A complex phase profile $\Phi = \frac{2\pi}{\lambda}(f - \sqrt{\rho^2 + f^2}) + \ell\varphi$ (f is the focal length) is required, each component can be modulated by dynamic and geometric phase independently [147, 148]. More complex multifunctional phase structures of a vortex beam also can be created via a hybrid phase plate. A vortex beam carrying Airy phase also called Airy-vortex beam was produced based on dynamic and geometric phases [149]. The Airy phase was generated by modulation of dynamic phase through a SLM, while the spiral phase was generated by geometric phase via a metasurface. For a right-hand circularly polarized beam passing through this system, the output beam $E_{out}(\rho, \varphi) = Ai(\rho, \varphi)e^{-i2\sigma q\varphi}|L\rangle$ ($Ai(\rho,\varphi)$ is a cubic phase in the Cartesian coordinates). The schematic of generating an Airy-vortex beam was shown in Figure 5A. The intensity profile of the Airy-vortex beam carrying topological charge $|\ell| = \pm 1$ for different handedness incident indicates the beam possessing both the Airy phase and spiral phase embedded in the wavefront. A single ultrathin hybrid metasurface generating an Airy and spiral phase via dynamic and geometric phase independently was able to produce an Airy-vortex beam [151]. The capability of encoding both the dynamic and geometric phases was also demonstrated to generate and split the vortex beams according to different SAM on a single ultrathin element [150, 152, 153]. The Panchartnam-Berry phase forms a phase gradient along the interface, manifested as the photonic spin Hall momentum offset [130–132, 135, 154]

$$\Delta k = \nabla\Phi_{PB}(x, y) = \sigma_i \frac{\partial\Phi_{PB}}{\partial x}\vec{e_x} + \sigma_i \frac{\partial\Phi_{PB}}{\partial y}\vec{e_y} \tag{4}$$

where σ_i is the SAM value of each photon after emerging from the interface, $\vec{e_x}$, $\vec{e_y}$ represent the unit vector in the corresponding directions. As an example, a metasurface fork grating was designed to split the spins and generate optical vortex simultaneously, as shown in Figure 5B.

3.3.3 Arbitrary spin-orbital angular momentum conversion

Optical vortex beams carrying orbital angular momentum generated via geometric phase metasurfaces arising

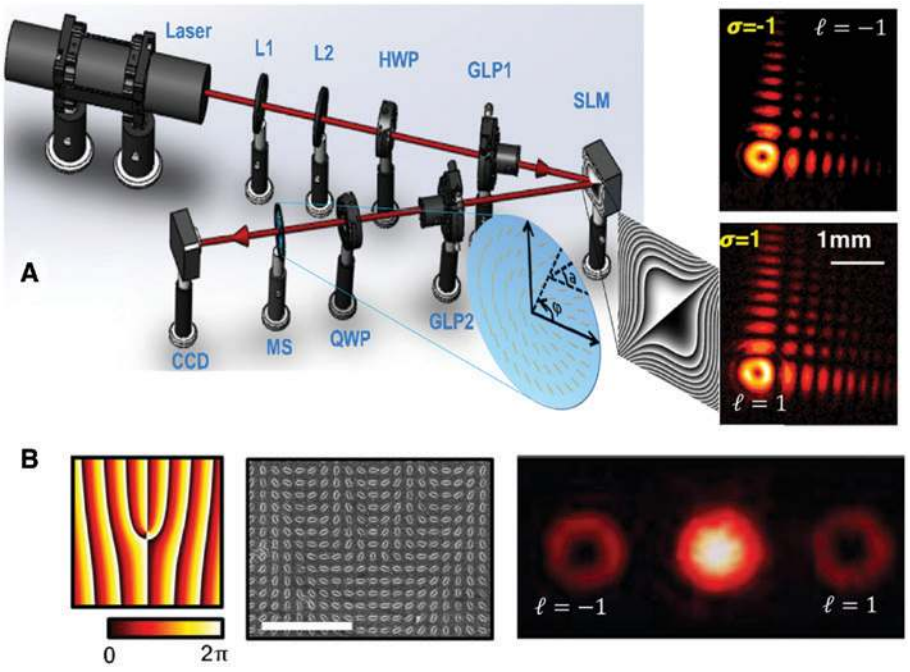

Figure 5: Multifunctional optical vortex generation by hybrid phase plates.
(A) Schematic and intensity profile of Airy-vortex beam generation by independent dynamic and geometric phase modulation. Reprinted from Ref. [149]. (B) A geometric phase metasurface hologram generates optical vortex beams and splits the spins simultaneously. Reprinted from Ref. [150].

from the spin-orbit interaction by the polarization manipulation have been demonstrated. When passing through a geometric phase plate with 100% polarization conversion efficiency, namely the phase retardation is $\delta=\pi$, the polarization states will be totally converted to its opposite states. Due to the rotational symmetric geometry, the output OAM states are constrained to be conjugated. The transformation process of a pair of orthogonal circularly polarized states passing through a geometric phase plate can be written as

$$\begin{cases} |\mathrm{R}\rangle \rightarrow \mathrm{e}^{-\mathrm{i}\ell_1\varphi}|\mathrm{L}\rangle \\ |\mathrm{L}\rangle \rightarrow \mathrm{e}^{-\mathrm{i}\ell_2\varphi}|\mathrm{R}\rangle \end{cases} \tag{5}$$

where $|\ell_1|=|\ell_2|$, $\mathrm{sign}(\ell_1)=-\mathrm{sign}(\ell_2)$. As a comparison, the spin-orbit interaction via rotationally symmetric dynamic phase manifests the transformation process in a similar way, with $|\mathrm{R}\rangle \rightarrow \mathrm{e}^{-\mathrm{i}\ell_1\varphi}|\mathrm{R}\rangle$, $|\mathrm{L}\rangle \rightarrow \mathrm{e}^{-\mathrm{i}\ell_2\varphi}|\mathrm{L}\rangle$ while $(\ell_1=\ell_2)$ without changing its polarization states and achieving a global OAM states. For any of each process, the OAM state is not independent. Once a phase plate was designed, either modulating the dynamic phase or geometric phase, the generated optical vortex after light passing through it carries same value of OAM ($\ell\hbar$) with same or opposite sign for a pair of orthogonal incident states. The Jones matrix of a dynamic phase plate and a geometric phase plate, neglecting the absorption and loss, are described as

$$\begin{cases} \mathrm{J_d}=\mathrm{e}^{\mathrm{i}\ell_\mathrm{d}\varphi}\begin{bmatrix}1 & 0\\ 0 & 1\end{bmatrix} \\ \mathrm{J_g}=\mathrm{R}(\theta)^{-1}\begin{bmatrix}1 & 0\\ 0 & \mathrm{e}^{\mathrm{i}\delta}\end{bmatrix}\mathrm{R}(\theta) \end{cases} \tag{6}$$

A possible way to break the bounding conditions to enable an arbitrary operation of OAM generation was proposed in 2008 [155]. By allowing light to pass through a system containing a geometric phase plate and a dynamic phase plate, independent OAM states were generated, as shown in Figure 6A. The output states from the system can be found as $|\mathrm{E_{out}}\rangle=\mathrm{J_dJ_g}|\mathrm{E_{in}}\rangle$. For the incident of right circularly polarized light $|\mathrm{R}\rangle$, the output is converted to $|\mathrm{L}\rangle$, with OAM $\ell=0$ and when the incident is left-hand circularly polarized $|\mathrm{L}\rangle$, the output converted to $|\mathrm{R}\rangle$ but carries OAM $\ell=1$. This process was further developed and implemented

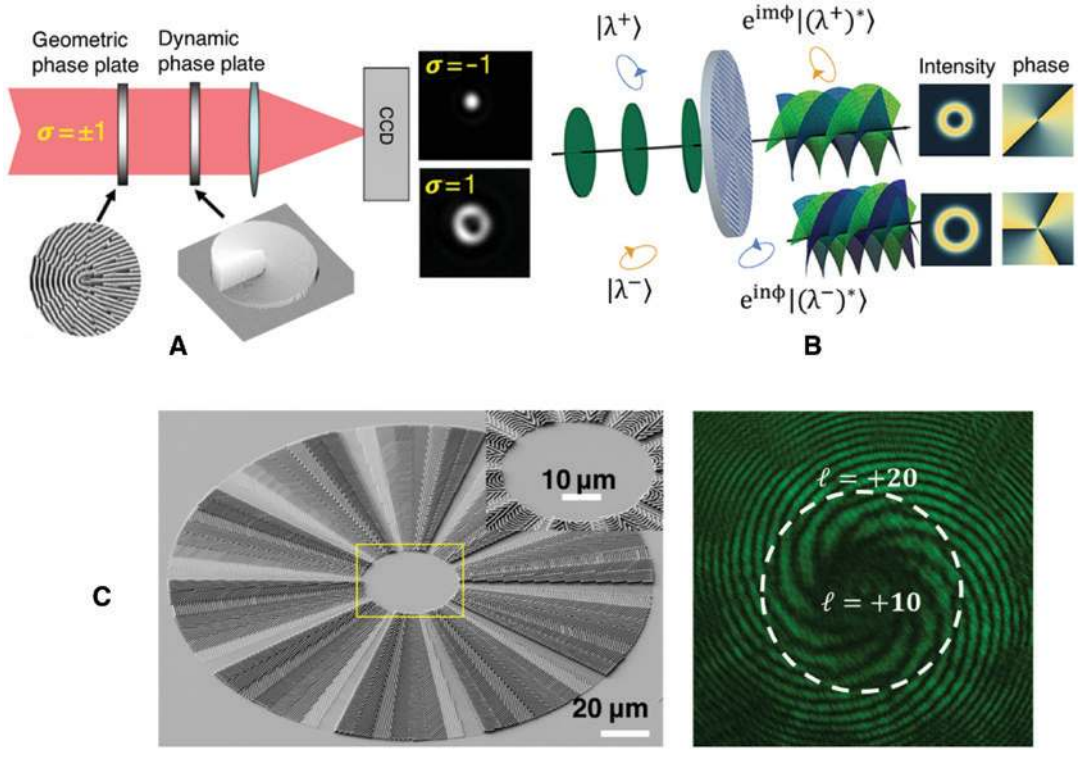

Figure 6: Independent spin-orbital angular momentum conversion by hybrid phase plate.
(A) Schematic illustration of independent spin-orbital angular momentum conversion of a pair of spin states passing a system consisted by geometric phase and dynamic phase plates. Reprinted from Ref. [155]. (B) Illustration of a hybrid metasurface plate for arbitrary OAM generation. Reprinted from Ref. [156]. (C) A hybrid dielectric metasurface plate fabricated by femtosecond laser printing generates $\ell=10$ for spin value $\sigma=-1$ and $\ell=20$ for spin value $\sigma=1$ simultaneously when illuminated by a linear polarized light. Reprinted from Ref. [157].

by a single metasurface which has a hybrid phase of dynamic and geometric phases, which enables any orthogonal pairs of input polarization states being converted to arbitrary pairs of OAM states [156–158]. This capability further improves the security for information encoding using OAM states [158, 159]. Figure 6B shows a schematic of a hybrid metasurface allowing independent OAM generation. A hybrid metasurface fabricated by femtosecond direct laser writing was also reported recently [157], which is able to generate arbitrary high orders of OAM states for different spin states, as shown in Figure 6C.

4 Active vortex laser

4.1 Free space optical vortex lasers

The first demonstration of vortex laser dates back to 2000. By inserting an SPP into laser cavity as a black reflector, as shown in Figure 7A, it introduces high losses to all other modes while it is almost lossless for the desired helical mode [160]. Since then, many approaches have been implemented for vortex laser creation using phase only [164, 165], amplitude only [166, 167], and phase amplitude combination [168] optical elements. For laser cavities based on amplitude-only optical elements, most of them are not capable of creating desired helical wavefront, but instead, they simultaneously produce two LG modes of opposite but equal azimuthal index, resulting in zero net OAM output. This kind of superposition of OAM modes have been demonstrated in many cavities with special elements, such as spot-defect mirrors [169], SLMs [161] as shown in Figure 7B, a pair of Porro prisms [167], aberrated lens [170], and angular light pumping profile [171].

A recent study shows that the handedness of OAM modes can be controlled by employing a novel mode selection element (MSE) consisting of two thin aluminium stripes, as shown in Figure 7C, which introduces higher loss for one helicity compared with the other [162]. According to this approach, the helicities of $\ell = \pm 1$ could be selected by adjusting the displacement of MSE. Another approach is to introduce a tilted etalon in laser cavity for OAM handedness selection [163], as shown in Figure 7D. This etalon is analogous to the Brewster windows, which is widely used for linear polarization selection in a laser cavity [172]. At a specific moment, vortex beams carrying opposite helicity have different twisted angle on the wavefront compared to each other. By adjusting the tilt angle of the etalon, more energy loss on the undesired handedness of OAM modes occurs, resulting in the survival of the only single handedness of vortex laser beam.

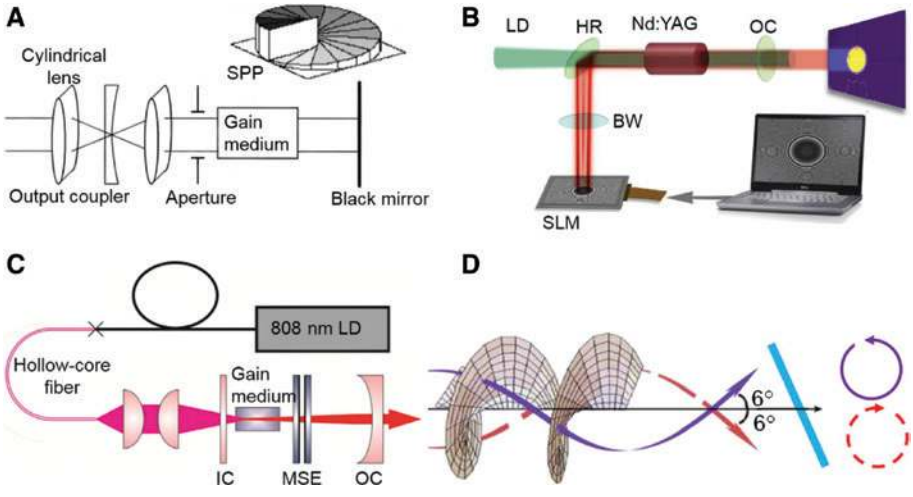

Figure 7: Vortex lasing from laser cavity.
(A) The first OAM laser resonator configuration, with spiral phase element (SPE) as black mirror. Reprinted from Ref. [160]. (B) Schematic of the digital laser composed of Brewster window (BW), spatial light modulators (SLMs), high reflectivity (HR) mirror at an angle of 45°, Nd:YAG gain medium pumped by an external laser diode (LD) source and the output coupler (OC). Also shown is a superposition of two Laguerre-Gaussian modes of opposite but equal azimuthal index, $l = \pm 25$. Reprinted from Ref. [161]. (C) Schematic of experimental laser setup for the handedness controlled Laguerre-Gaussian (LG01) mode, with a pair of mode-selection element (MSE), input coupler (IC), output coupler (OC) and Nd:YAG gain medium. Reprinted from Ref. [162]. (D) Schematic description of the concept of using Poynting vector skew angle to introduce energy loss discrimination based on the Poynting vector of Laguerre-Gaussian (LG) modes along the propagation direction. The tilted bar on the path is the etalon and the purple solid circle/red dash circle indicates the trajectory of the Poynting vector LG mode of different handedness. Reprinted from Ref. [163].

Optical vectorial vortex beams carrying a singularity on its phasefront with spatially inhomogeneous polarization states were found have many potential applications [173], [174]. These beams possessing arbitrary polarization and OAM states can be mapped over a higher-order Poincaré sphere (HOP), as shown in Figure 8A [175], which is an analogue to the Poincaré sphere for polarization and the Bloch sphere for OAM [176]. Vectorial vortex beams can be created based on spin-orbit interaction when light passing through inhomogeneous anisotropic medium [65, 137, 141, 177], being tightly focused [178] or being coupled into nanowaveguides where light is strongly confined in the transverse direction [179–182]. HOP sphere beams have been directly produced from laser cavities with high purity [67]. By inserting a pair of geometric phase plates to convert OAM modes to circularly polarized Gaussian modes and vice versa, assisting with a pair of quart-wave plate for full polarization control, vector vortex modes are generated in that laser cavity, as shown in Figure 8B.

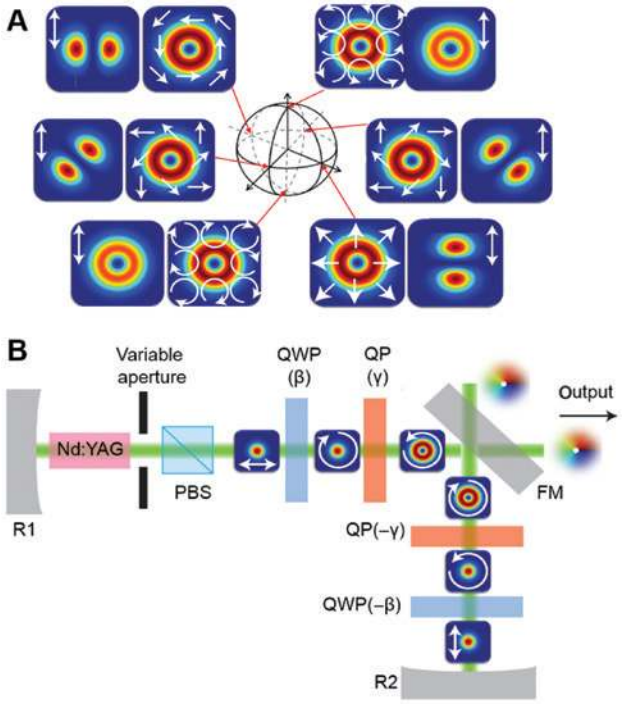

Figure 8: Vectorial vortex lasing.
(A) Vertex beams of various polarization described by the higher-order Poincaré (HOP) sphere. The white arrows show each beam's polarization. These beams have different spatial distribution after passing through a linear polarizer oriented in the vertical direction, as depicted by the double-ended arrows. (B) Conceptual description of the experiment setup where mirrors R1 and R2 together form the Fabry-Perot lasing cavity. The selection of OAM relies on the spin to orbital AM coupling provided by the q-plates. Changing the orientation angle (β) of the first quarter-wave plate (QWP) and the rotating angle of the first q-plate (QP) results in different OAM polarization states on the HOP sphere. An additional QWP and a second QP are also required to convert the vector OAM mode into a linearly fundamental Gaussian mode. Thus, the polarization and OAM mode at each position repeat themselves over a cavity round trip. Reprinted from Ref. [67].

The OAM lasers discussed above are continuous wave (CW) lasers. However, an optical vortex pulsed laser with Q-switched operation [183] and self-mode-locked Laguerre-Gaussian lasers with tunable OAM output was also demonstrated [184].

4.2 Integrated OAM lasers

Alone with recent advances in the field of nanofabrication and engineered optical materials, the integration of devices has become the inevitable trend of modern photonics. There is an increasing demand on the realization of vortex lasing on an integrated chip. Integrated optical vertex lasing can be implemented by adding an integratable vortex generator element at the output port of light source or generating vortex beam inside the light source cavities directly. A micro-vortex laser was implemented by employing a micro-SPP on the output port of a vertical cavity surface emitting laser [185], as shown in Figure 9A. A significant advance towards integrated OAM solution is the experiment demonstration of miniature optical vortex emitters based on silicon micro rings with angular grating patterns (see in Figure 9B) [186]. This emitter is able to generate vortex with well-controlled amount of OAM. For the clockwise (or anti-clockwise) Nth order whispering gallery modes (WGMs) supported in a micro silicon ring, its energy get scattered by the angular grating sidewall (M equidistant scatters), resulting in OAM scattering light as output with an OAM amount of $\ell\hbar$, where $\ell = N - M$. Despite its compact footprint and accuracy in phase control, the resonance feature of WGMs introduces an undesired disadvantage, that is, intrinsic narrow band operation. To overcome this bandwidth limitation, recently, an ultra-broadband multiplexed OAM emitter is proposed and experimentally demonstrated [187], as shown in Figure 9C. It utilizes the global optimization algorithm to design the free-form metasurfaces to obtain a spiral phase for the output beam. The operation bandwidth of this device is as wide as 200 nm at optical communication wavelengths around $\lambda = 1550$ nm. Moreover, the device itself is reciprocal and thus it can be used for OAM demultiplexing, routing the ±1 order of OAM into opposite direction respectively in silicon waveguides.

In paraxial regime, circularly polarized beams carry SAM only. However, in non-paraxial circumstances, where the circularly polarized light is strongly confined in the

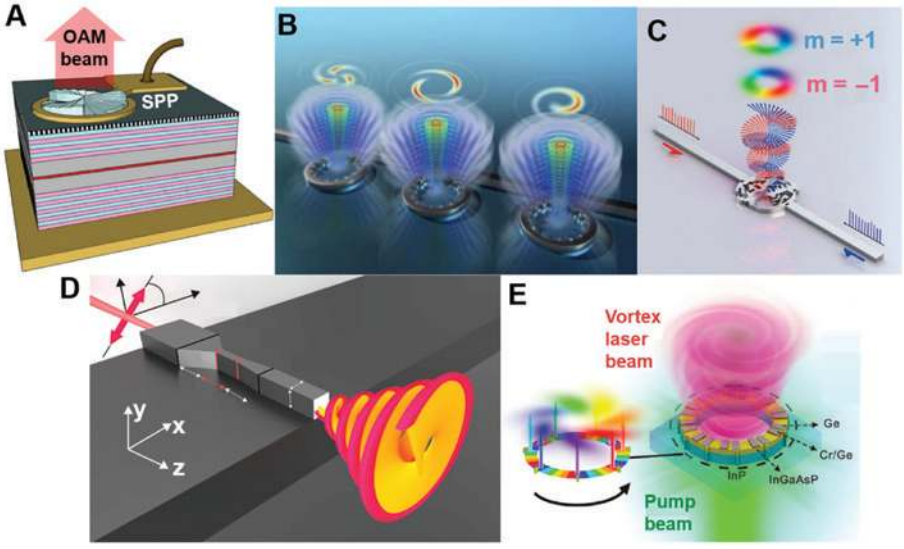

Figure 9: Micro-vortex lasing on chip.
(A) Schematic of the vertical-cavity surface-emitting laser with an integrated spiral phase plate at the output port. Reprinted from Ref. [185]. (B) Schematic of integrated optical vortex emitters based on silicon waveguides. The angular grating patterns scatter OAM light as output in free space. Reprinted from Ref. [186]. (C) Schematic of a broadband OAM emitter which can also be used for OAM multiplexing and demultiplexing. Reprinted from Ref. [187]. (D) Sketch of an integrated AlGaAs waveguide device and its generation of OAM by spin to orbital AM conversion. Reprinted from Ref. [188]. (E) Schematic of an OAM microlaser on an InGaAsP/InP platform. The on-top Ge and Cr/Ge introduce different loss and gain modulations so they form an exceptional point operation which allows for one-way light circulation in the micro ring cavity. It emits a vortex laser beam under optical pumping. Reprinted from Ref. [189].

transverse direction, the confined circularly polarized beams carry both SAM and OAM [134, 178]. Nanophotonic waveguides provide strong confinement of light in the transverse direction. Therefore, generating circularly polarized light in nanophotonic waveguides yields a confined circularly polarized mode with a strong longitudinal OAM component. This idea was theoretically proposed in 2014 [181, 190] and recently demonstrated in experiment [188]. By introducing asymmetric geometry of the structure in nanoscale, nanophotonic waveguides exhibit considerable birefringence. By introducing a phase lag of $\pi/2$ between the transverse electric and transverse magnetic modes, a confined circularly polarized mode in deep subwavelength waveguides was generated. A strong longitudinal OAM component was also found in this mode due to SAM to OAM conversion, as shown in Figure 9D. Manipulation of confined circularly polarized modes on a chip leads to many phenomena and applications, such as optical meshing gears [182] and chirality beam splitters [191].

As mentioned above, a micro-ring resonator with angular grating patterns can generate well-control amount of OAM. However, the OAM mode is spin dependent. The micro-ring resonator with angular grating patterns produces a scattering light beam with $\sigma\ell\hbar$ OAM. In micro-ring cavity lasers, clockwise and counter-clockwise WGMs will be simultaneously excited due to the mirror symmetry of a ring cavity. As a consequent, zero net OAM scatters from the output. Therefore, the bidirectional excitation of WGMs poses a significant challenge for integrated OAM micro-ring lasers. In conventional ring cavity lasers, it usually requires the employment of isolators to achieve unidirectional operation [192, 193]. However, the realization of isolators requires for the breaking of reciprocity, which is extremely challenging in nano- or microscale [194, 195]. Recent advances in the field of non-Hermiticity shows that exceptional points can break the limitation of bidirectional excitation in micro-ring lasers [196, 197]. By introducing complex refractive index modulations (with periodic loss-gain distribution along the azimuthal direction) to form an exceptional point, researchers realized the unidirectional power circulation in a micro-ring laser [189], as shown in Figure 9E. Thus, the micro ring with angular gratings allows for only one direction of light circulation, resulting in integrated OAM laser emission.

5 Fractional-order OAM beam generation

Hitherto, the approaches for fractional-order OAM generation are primarily concerned with two branches: direct

output from a laser resonator cavity and external-cavity conversion. The latter recipe encompasses non-integer spiral phase plate [198–200], computer-generated holograms [201, 202], generic superposition of beam modes [203, 204] internal conical diffraction [205], high harmonic generation [206], propagation-induced radial phase gradient [207], or generalized differential operator [208]. Accordingly, several avenues, including mode transformation [209], reverse mode sort [210] and a pair of cylindrical lens [211], have been established to realize the detection of fractional-order OAM.

Similar to the light beams carrying integer OAM, the conceptually simplest method to yield a fractional-order vortex beam outside the cavity is the facile usage of the spiral phase plate with fractional step height [198–200]. The topological charge value can be flexibly navigated in principle by controlling over the relevant step height with very high accuracy. Alternatively, an elaborated holographic technique can also be exploited for synthesis of the optical beams possessing fractional vortices [201, 202]. This realization is responsible for a half-cut phase ramp that is encoded to the helically phase hologram for giving birth to a spatially distinct sub-harmonic diffracted fractional OAM beams. What one should pay attention to is the instability of these types of helical beams upon propagation according to the aforementioned methods. In response to this scenario, a feasible route, the coherent synthesis of Laguerre-Gaussian modes with diverse topological charge values, has been proposed to produce light beams with fractional OAM. It is able to enhance propagation stability in this way by limiting the number of different Gouy phases in the superposition [204]. Moreover, another interesting fashion called internal conical diffraction in the biaxial crystal is utilized to convert an elliptically polarized light into a light beam with continuously tunable fractional OAM in the range 0 to1$\hbar$ per photon [205]. To extend the applicability of the fractional OAM beams by this technique, high-order harmonic generation with infrared conical refraction beams has been proved to an efficient method to achieve half-integer OAM beams in the extreme ultraviolet domains [206].

In a different front, new conversion mechanisms from integer vortices to non-integral ones is highly desired to generalize the widespread applications of the fractional-order OAM beams. It was suggested that making use of the propagation-triggered radial phase gradient of initial Laguerre-Gaussian beam is an excellent choice to dynamically sculpture plasmonic vortex from integer to fractional OAM. More importantly, an explicit analytical representation for the fractional vortex can be derived as a coherent superposition of numerous integer vortices [206]. Quite generally, a spiniform phase-encoded device comprising bilaterally symmetric with an aperture is put forward to yield arbitrary rotational-order vortex beams carrying OAM. This unique approach enables the rich quantum entanglement and superposition between arbitrary rational-order OAM light fields, leading to unprecedented quantum communication with low cross-talks [111].

On the other hand, fractional-order vortex beams associated with the Gaussian mode can also be created by taking advantage of intra-cavity approaches. The capability of producing Hermite–Laguerre–Gauss modes with a fractional-order OAM was proved by virtue of an astigmatic mode converter [212]. Recently, the nonplanar elliptical modes possessing large fractional OAM with transverse patterns revealing multiple spots near the degenerate cavities were excited by using a diode-pumped solid-state laser with selective pumping. It is also found that spatial distributions of these elliptical modes can be perfectly reconstructed theoretically, enabling analysis of the average OAM and the vortex structures [213].

6 Multiple optical vortex beam generation

6.1 OAM multiplexing

Among all bulk optic versions, using modified interferometric configurations is perhaps the most routine one, owing to their capability to control over the array density and position of vortices in real time [214]. As an alternative, diffractive optical elements can be purposefully engineered to emulate almost any refractive holographic element for multiplexing the OAM vortices into an array [215, 216]. What makes this approach particularly fascinating is because of commercially available pixelated SLMs. In this regard, the generated multiple OAM beams carrying desired topological charges can be readily configured by dynamically updating the incident phase/amplitude patterns loaded on the SLMs. More impressively, binary phase Dammann optical vortex gratings through hologram coding are demonstrated to offer a viable solution for the multiplexing of massive OAM channels with uniform energy distributions and enlarged vortex-detection capabilities [217], as shown in Figure 10A. With regard to the OAM division multiplexing for ultrahigh-speed and large-capacity optical communications, Dammann optical vortex gratings can work as key ingredients to yield multiple OAM channels, multiplex these channels

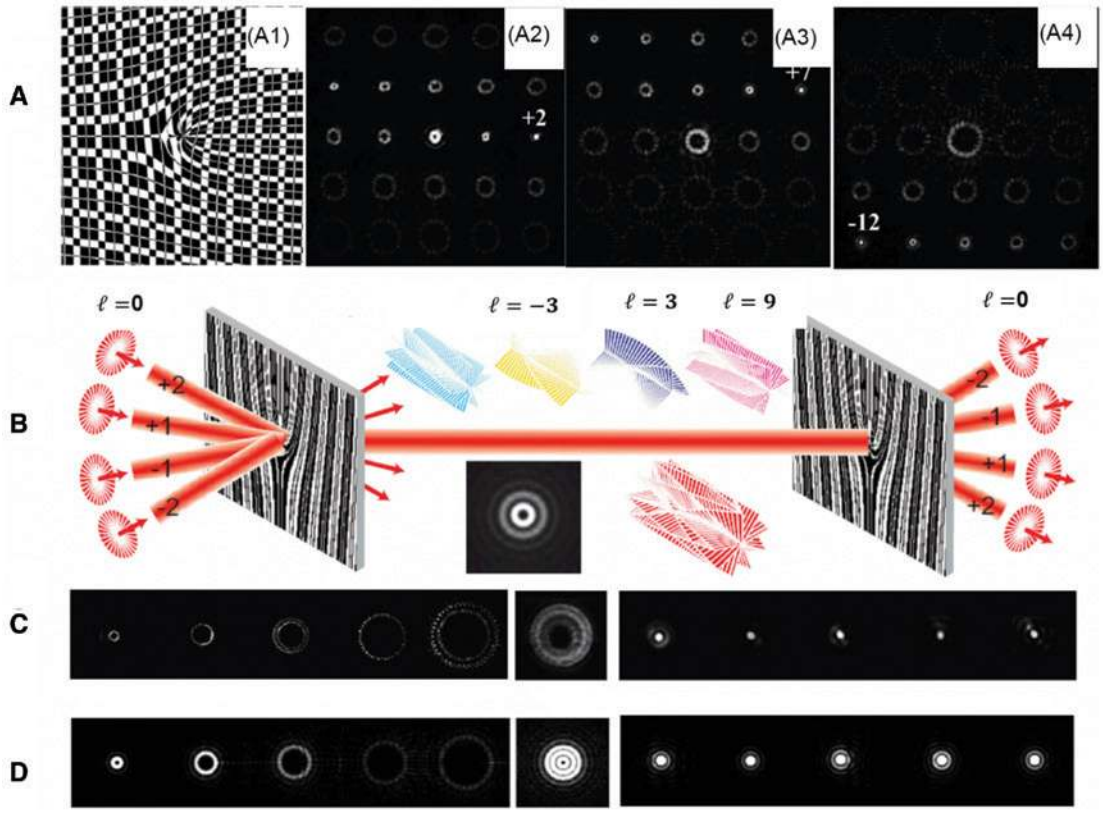

Figure 10: OAM multiplexing via Dammann gratings.
(A1) Phase pattern of 2D Dammann vortex grating (black for 0 and white for π); (A2)–(A4) optical vortex with various topological charges (−2, −7, and 12) detection by the Dammann vortex grating. Reprinted from Ref. [217]. (B–D) Schematic of OAM-based free-space optical communications using the Dammann optical vortex grating for multiplexing/demultiplexing. Reprinted from Ref. [218].

into coaxial OAM beams, as well as separate them equally for the demultiplexing process (see Figure 10B–D) [218].

Mode-sorting multiplexing approach was first pioneered to sort OAM states of light [219] and then exploited to improve the separation efficiency of the OAM beams [220]. Furthermore, a robust technique that integrates interferometry with conjugate helical phase elements directing OAM beams onto a series of output ports, has been demonstrated to implement on-chip noninterference angular momentum (including SAM and OAM) multiplexing of broadband light. Toward achieving this, coaxially superposed light beams with four angular momentum states pass through a mode-sorting nanoring aperture multiplexing unit consisting of shallow nanogrooves and the spatially shifted mode sorting nanoring slits of variant sizes. In light of the angular momentum mode-sorting principle, on-chip multiplexing of multiple OAM modes can be formed. The nonresonance mode-sorting attribute is also able to enlarge the multiplexing capacity in conjunction with the wavelength-division multiplexing over a bandwidth of 150 nm [221]. Moreover, high-capacity millimetre-wave communications with well-defined spectral efficiency have been testified using four OAM multiplexing. It is noteworthy that, at the OAM demultiplexer stage, the intensity distribution of four diverse OAM beams in the desired sorting direction is detected, suggesting that the multiplexed OAM beams are spatially separated by the OAM mode demultiplexer [222].

6.2 OAM multicasting

In addition to OAM multiplexing, multicasting where generates multiple coaxial OAMs from a single input, has also been desired from the perspective of efficient optical signal processing in one-to-many communications, which speeds up the end users to acquire the duplicate data, by replicating data into orthogonal multiple channels in the optical domain. Currently, optical multicasting is required in many optical communication applications, such as teleconferencing, interactive distance learning, video distribution, live auctions, and distributed computing.

The SLMs loaded with specially designed phase pattern can be used to realize OAM multicasting. Using

a sliced phase pattern, multicasting data from a single OAM spatial channel onto multiple OAM channels of equally spaced OAM charge numbers was demonstrated [223]. A pattern search assisted iterative (PSI) algorithm was proposed to enable simultaneous generation of multiple OAM modes using a single phase-only element. Generating 100 randomly spaced OAM modes with high diffraction efficiency, low standard deviation and low relative root-mean-square error has been achieved via the PSI algorithm [224]. Metasurface structure with a V-shaped antenna array can be also used to realize on-chip multicasting from a single Gaussian beam to multiple OAM beams [225]. The shared aperture technology has been shown to be capable of performing a series of concurrent tasks, representing a new paradigm for the design of innovative photonic devices with improved functionality [226, 227]. However, it is might be valuable to unite the shared aperture principle with the geometric phase metasurface that offers a feasible roadmap to realize multifunctional planar configurations. Thereinto, the photonic geometric phase metasurface possessing interleaved phase profiles are judiciously engineered by mixture of optical nanoantenna sub-arrays. The principle of this scheme is that exploits the exotic capability of random patterns to realize multiple OAMs and executes polarization helicity control through the geometric phase layout. It has been proposed that there exists twofold possible routes to design shared-aperture-assisted metasurfaces yielding multiple spin-dependent OAM beams. On the one hand, multiple vectorial vortices are enabled to be achieved by coherent superposition of wavefronts with opposite chiralities using interleaved geometric phase metasurface. For another, the alliance of the harmonic response and geometric phase concept is utilized to obtain the spin-dependent diffraction pattern consisting of multiple OAM harmonic orders with opposite circularized polarization illuminations [129, 228].

Moreover, feedback-assisted adaptive multicasting from a single Gaussian mode to multiple OAM modes with adjustable power weight coefficients was demonstrated using a complex phase pattern [229]. Additionally, OAM multicasting by arbitrary manipulation of spatial amplitude and phase, turbulence compensation of distorted OAM multicasting by adaptive optics, obstruction-free data-carrying N-fold Bessel modes multicasting from a single Gaussian mode, and data-carrying OAM-based underwater wireless optical multicasting link were also demonstrated [230–233], show favourable performance of OAM multicasting and its wide applications.

6.3 Optical vortex array

An OAM-carrying optical vortex is an isolated point singularity (e.g. phase) of an optical field. A network of optical vortices, also called optical vortex array or optical vortex lattice, has also caught widespread attention owing to some distinct properties compared to isolated ones. For instance, the shift of optical vortex lattice has been applied to the measurement of small-angle rotations and small linear displacements, reconstruction of wavefront geometry, and three-dimensional scanning interferometry. Moreover, the optical vortex lattice has also found interesting applications in the manipulation of micro-optomechanical pumps, microlithography, nonlinear propagation of phase singularity array, and quantum processing.

There are several approaches for generating optical vortex array, such as hologram [215], transformation of Laguerre-Gaussian mode [234], sematic liquid crystals [235], and multi-plane-wave interferometer [7]. These schemes rely on a number of bulky diffractive optical elements with relatively large volume and long working distance. An alternative approach is to use photonic integrated devices with small footprint. A simple and compact on-chip optical vortex lattice emitter on the silicon photonics platform was recently demonstrated [236]. The principle relies on the three-plane-wave interference. The on-chip optical vortex lattice emitter consists of three parallel waveguides with etched tilt gratings. The tilt gratings facilitate flexible light emission in a wide range of directions, enabling the generation of optical vortex lattice above the silicon chip. A network of dark spots and fork-like fringe patterns observed in the experiment confirm the on-chip optical vortex lattice emission. The demonstrations with favourable performance may open a door to generate, manipulate and detect optical vortex lattice using silicon photonic integrated circuits.

Optical vortex beam arrays with spatially variant topological charge have been generated by peculiar patterned metasurfaces [237–241]. A nanoslit metasurface has been designed that is able to produce multi-channel OAM beams along with equal energy in each channel at a wavelength of 632.8 nm, as schematically illustrated in Figure 11A. The ultrathin multiple OAM beam generator consists of an array of nanoantennas (i.e. a 6×6 beam generator in Figure 11B), whose the geometry and orientation was cautiously engineered to simultaneously manipulate both phase and amplitude. Using the principle of holography, the phase and amplitude information of the multiple OAM beam array can be acquired, and then encoded to the spatial orientation and geometry of the antenna. In

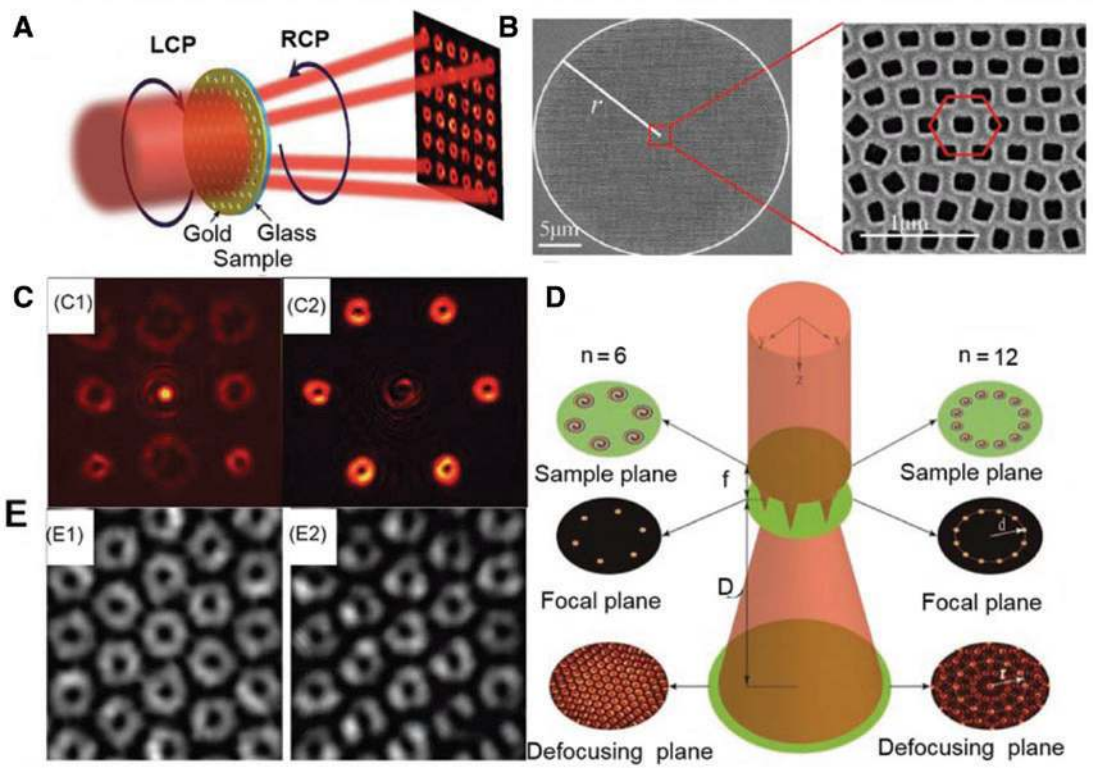

Figure 11: Optical vortex arrays generated via planar metasurfaces.
(A) Illustration of the multi-channel vortex beam generation enabled by a metasurface. (B) SEM picture of the 6 × 6 OAM beam generator. (C) Multi-channel OAM beams with various topological charges (C1) and hexagonal profile (C2). Reprinted from Ref. [240]. (D) Illustration of the principle on the quasi-Talbot effect of OAM beams whose centers are placed in a rotationally symmetric position. (E) Numerical (E1) and experimental (E2) results of the vortex array by the predesigned metasurface on the defocusing plane. Reprinted from Ref. [241].

this fashion, multi-channel OAM beams with different topological charges and well-defined hexagonal array can be accessible [240], as shown in Figure 11C. To further increase the amount of OAM beams, the quasi-Talbot effect of vortex foci for generation of optical vortex arrays by metasurface was demonstrated. The quasi-Talbot effect of OAM beams in which centers are placed in a rotationally symmetric position was utilized to design the metasurface, as shown in Figure 11D. By arranging the positions of OAM lenses, formed with anisotropic nano-apertures, the metasurface-dependent device can create and focus the multiple vortex beams carrying OAM on the focal plane, thus enabling optical vortex arrays consisting of dozens of hollow spots on the defocusing plane, as shown in Figure 11E [241].

7 Conclusions and perspectives

Light fields carrying OAM have opened new perspectives in the optical research realm due to a synergy of several fascinating attributes. We have briefly reviewed the latest developments in the field of optical vortex generation toward to the trend on compactness, high integration. The advanced nanofabrication technology enables the design and fabrication of planar phase elements to modulate the wavefront in microscale and nanoscale. By engineering the optical path to modify phasefront based on the propagation effect, polarization independent optical vortex beams can be generated. Metasurfaces based on metallic or dielectric resonant nanostructures offer an excellent flexibility to generate optical vortex beams via resonant tuning or polarization manipulation, within an infinitesimal dimension. The independent modulation of these two kinds of phase gives rise to the multifunctional optical vortex generation and unconjugated OAM states manipulation. Direct creating a vortex source rather modifying the beam path by inserting a discrete component, is thought to be a further improvement not only the level of integration and compactness, but also the purity of the vortex mode. Fractional optical vortex carrying fractional OAM are able implement via discrete plates or in laser cavities. Generating multiple vortex beams from a single

device makes it more fascinating. The technologies on multiplexing, multicasting and vortex array generation have been briefly reviewed. We intend by presenting these works together in a concise and coherent way to stimulate further research progress on vortex beam generation in optics and as well as other forms of waves. We believe the similar design methods and approaches on optical vortex generation summarized here will benefit the communities in electron vortex, neutron vortex, acoustic and microwave vortex generation and applications.

However, different approaches have their own limitations. Discrete planar plates are suffering low purity of the desired beams, attributed from diffraction effect, especially high order vortex generation, no matter they are dynamic, geometric or hybrid phase metasurfaces. While for geometric phase plates, the purity of the desired vortex is much more sensitive to the dichroism of the material and structure, and the retardation. Engineering the laser cavity in free-space or design novel waveguides lead to vortex lasing with a high mode purity. However, the challenge still hinders its way on the development of vortex lasers, because of the difficulty on handedness selection of the resonant modes arising from the rotational symmetry of the laser cavity. Moreover, higher orders are hard to generate by laser cavities and waveguides. Another property to consider is the bandwidth of the device on the resonant frequency. Vortex laser has an intrinsic ultra-narrow bandwidth comparing to the dynamic phase metasurfaces. Furthermore, the difficulty on generating high order vortex beams has to be taken into consideration for different approaches. It is much difficult to generate high order vortex via laser cavities or waveguides, due to the physical limitations of the cavity and waveguide dimension. Vortex beams carrying hundreds of OAMs have been realized by centimeter-scale SPPs and high resolution SLMs, while metasurfaces fabricated by electron-beam lithography or ion-beam lithography are not practical for large order vortex generation, due to the fabrication process are low throughput and cost-ineffective. Vortex metasurfaces fabricated via femtosecond laser 3D printing techniques, which bridges the nanoscale to macroscale, are promising to cope with this challenge. High order vortex beams have been achieved from a geometric phase plate with 200 μm in diameter. The well-known high throughput of this fabrication technique opens the door toward to high order optical vortex generation. Which makes this technique more fascinating is its capability of 3D writing on any type of surfaces and substrates, multifunctional and high order optical vortex beams are able to generate from a high-integrated device or optical system. The utilization of reconfigurable materials enable the possibility to switch different order of vortex beams in real-time, which make it possible to design a functional device with more flexibility and tenability.

Acknowledgments: X. W. Wang acknowledges the partial support from the Swinburne Research Institute Seed Fund Grant, the Swinburne ECR-SUPRA Award program, and the Swinburne FSET-ECR Award. Z. Nie acknowledges the support from the National Natural Science Foundation of China (No. 11274106). J. Wang thanks the support from the National Natural Science Foundation of China (No. 11574001, No. 61761130082, and No. 11774116), the National Basic Research Program of China (973 Program; No. 2014CB340004), the Royal Society-Newton Advanced Fellowship, the National Program for Support of Top-notch Young Professionals, the Natural Science Foundation of Hubei Province of China (2018CFA048), and the Program for HUST Academic Frontier Youth Team. T. Li thanks the support from the National Natural Science Foundation of China (No. 11674167) and Dengfeng Project B of Nanjing University.

References

[1] Nye JF, Berry MV. Dislocations in wave trains. Proc R Soc A 1974;336:165–90.
[2] Verbeeck J, Tian H, Schattschneider P. Production and application of electron vortex beams. Nature 2010;467:301–4.
[3] Yang Y, Thirunavukarasu, Babiker M, Yuan J. Orbital angular momentum modes seletion by rotationally symmetric superposition of chiral states with application to electron vortex beams. Phys Rev Lett 2017;119:094802.
[4] Clark CW, Barankov R, Huber MG, Arif M, Cory DG, Pushin DA. Controlling neutron orbital angular momentum. Nature 2015;525:504–6.
[5] Baranova NB, Mamaev AV, Pilipetsky NF, Shkunov VV, Zeldovich BY. Wavefront dislocations: topological limitations for adaptive systems with phase conjugation. J Opt Soc Am 1983;73:525–8.
[6] Masajada J, Boguslawa D. Optical vortex generation by three plane wave interference. Opt Comm 2001;198:21–7.
[7] O'Holleran K, Padgett MJ, Dennis MR. Topology of optical vortex lines formed by the interference of three, four, and five plane waves. Opt Express 2006;14:3039–44.
[8] O'Holleran K, Dennis MR, Padgett MJ. Topology of light's darkness. Phys Rev Lett 2009;102:143092–4.
[9] Dennis MR, King RP, Jack B, O'Holleran K, Padgett MJ. Isolated optical vortex knots. Nat Phys 2010; 6:118–21.
[10] Indebetouw G. Optical vortices and their propagation. J Mod Opt 1993;40:73–87.
[11] Basistiy IV, Bazhenov VY, Soskin MS, Vasnetsov MV. Optics of light beams with screw dislocations. Opt Comm 1993;103:422–8.
[12] Basistiy IV, Soskin MS, Vasnetsov MV. Optical wavefront dislocations and their properties. Opt Comm 1995;119:604–12.

[13] Soskin MS, Gorshkov VN, Vasnetsov MV, Malos JT, Heckneberg NR. Topological charge and angular momentum of light beams carrying optical vortices. Phys Rev A 1997;56:4064–75.
[14] Rozas D, Law CT, Swartzlander GA. Propagation dynamics of optical vortices. J Opt Soc Am B 1997;14:3054–65.
[15] Bouchal Z. Resistance of nondiffracting vortex beam against amplitude and phase pertubations. Opt Comm 2002;210:155–64.
[16] Gbur G, Tyson RK. Vortex beam propagation through atmospheric turbulence and topological charge conservation. J Opt Soc Am A 2008;25:225–30.
[17] Allen L, Beijersbergen MW, Spreeuw RJC, Woerdman JP. Orbital angular momentum of light and the transformation of Laguerre-Gaussian laser modes. Phys Rev A 1992;45:8185–90.
[18] Coullet P, Gil L, Rocca F. Optical vortices. Opt Comm 1989; 73:403–8.
[19] Beijersbergen MW, Spreeuw RJC, van der Veen H, Woerdman JP. Astigmatic laser mode converters and transfer of orbital angular momentum. Opt Comm 1993;96:123–32.
[20] Beijersbergen MW, Coewinkel RPC, Kristensen M, Woerdman JP. Helical wavefront laser beams produced with a spiral phaseplate. Opt Comm 1994;112:321–7.
[21] Leach J, Padgett MJ, Barnett SM, Franke-Arnold S, Courtial J. Measuring the orbital angular momentum of a single photon. Phys Rev Lett 2002;88:2579011–14.
[22] O'Neil AT, MacVicar I, Allen L, Padgett MJ. Intrinsic and extrinsic nature of the orbital angular momentum of a light beam. Phys Rev Lett 2002;88:536001–14.
[23] Curtis JE, Grier DG. Structure of optical vortices. Phys Rev Lett 2003;90:1339011–4.
[24] He H, Friese MEJ, Heckenberg NR, Rubinsztein-Dunlop H. Direct observation of transfer of angular momentum to absorptive particles from a laser beam with a phase singularity. Phys Rev Lett 1995;75:826–9.
[25] Simpson NB, Dholakia K, Allen L, Padgett MJ. Mechanical equivalence of spin and orbital angular momentum of light: an optical spanner. Opt Lett 1997;22:52–4.
[26] Paterson L, MacDonald MP, Arlt J, Sibbett W, Bryant PE, Dholakia K. Controlled rotation of optically trapped microscopic particles. Science 2001;292:912–4.
[27] Padgett M, Bowman R. Tweezers with a twist. Nat Photon 2011;5:343–8.
[28] Padgett MJ. Orbital angular momentum 25 years on. Opt Express 2011;25:11265–74.
[29] Franke-Arnold S, Allen L, Padgett MJ. Advances in optical angular momentum. Laser Photon Rev 2008;2:299–313.
[30] Dholakia K, Čižmár T. Shaping the future of manipulation. Nat Photon 2011;5:355–42.
[31] Gibson G, Courtial J, Padgett MJ, et al. Free-space information transfer using beams carrying orbital angular momentum. Opt Express 2004;12:5448–56.
[32] Paterson C. Atmospheric turbulence and orbital angular momentum of single photons for optical communication. Phys Rev Lett 2005;94:1539011–4.
[33] Wang J, Yang JY, Fazal IM, et al. Terabit free-space data transmission employing orbital angular momentum multiplexing. Nat Photon 2012;6:488–96.
[34] Bozinovic N, Yue Y, Ren Y, et al. Terabit-scale orbital angular momentum mode division multiplexing in fibers. Science 2013;340:1545–8.
[35] Yin JY, Ren J, Zhang L, Li H, Cui TJ. Microwave vortex beam emitter based on spoof surface plasmon polaritons. Laser Photon Rev 2018;12:1600316.
[36] Mair A, Vaziri A, Weihs G, Zeilinger A. Entanglement of the orbital angular momentum states of photons. Nature 2001;412:313–6.
[37] Molina-Terriza G, Torres JP, Torner L. Management of the angular momentum of light: preparation of photons in multidimensional vector states of angular momentum. Phys Rev Lett 2002;88:136011–4.
[38] Fickler R, Lapkiewicz R, Plick WN, et al. Quantum entanglement of high angular momenta. Science 2012;338:640–3.
[39] Nagali E, Sciarrino F, De Martini F, et al. Quantum information transfer from spin to orbital angular momentum of photons. Phys Rev Lett 2009;103:136011–4.
[40] Fürhapter S, Jesacher A, Barnet S, Ritsch-Marte M. Spiral phase contrast imaging in microscopy. Opt Express 2005;13:689–94.
[41] Jack B, Leach J, Romero J, et al. Holographic ghost imaging and the violation of a bell inequality. Phys Rev Lett 2009;103:0836021–4.
[42] Li L, Li F. Beating the Rayleigh limit: orbital angular moment based super-resolution diffraction tomography. Phys Rev E 2013;88:332051–6.
[43] Toyoda K, Takahashi F, Takizawa S, et al. Transfer of light helicity to nanostructures. Phys Rev Lett 2013;110:1436031–5.
[44] Hamazaki J, Morita R, Chujo K, Kobayashi Y, Tanda S, Omatsu T. Optical vortex laser ablation. Opt Express 2010;18:2144–51.
[45] Hnatovsky C, Shvedov VG, Krolikowski W, Rode AV. Materials processing with a tightly focused femtosecond laser vortex pulse. Opt Lett 2010;35:3417–9.
[46] Courtial J, Dholakia K, Robertson DA, Allen L, Padgett MJ. Measurement of the rotational frequency shift imparted to a rotating light beam possessing orbital angular momentum. Phys Rev Lett 1998;80:3217–9.
[47] Lavery MPJ, Speirits FC, Barnett SM, Padgett MJ. Detection of a spinning object using light's orbital angular momentum. Science 2013;341:537–40.
[48] Litchinitser NM. Structured light meets structured matter. Science 2012;337:1054–5.
[49] Korech O, Steinitz U, Gordon RJ, Averbukh IS, Prior Y. Observing molecular spinning via the rotational Doppler effect. Nat Photo 2013;7:711–4.
[50] Swartzlander GA, Ford EL, Abdul-Malik RS, et al. Astronomical demonstration of an optical vortex coronagraph. Opt Express 2008;16:10200–7.
[51] Tamburini F, Thidé B, Molina-Terriza G, Anzolin G. Twisting of light around rotating black holes. Nat Phys 2011;7:195–7.
[52] Qiu CW, Yang Y. Vortex generation reaches a new plateau. Science 2017;357:645.
[53] Wang XW, Kuchmizhak AA, Li X, et al. Laser-induced translative hydrodynamic mass snapshots: noninvasive characterization and predictive modelling via mapping at nanoscale. Phys Rev Appl 2017;8:440161–7.
[54] Yu N, Capasso F. Flat optics with designer metasurfaces. Nat Mater 2014;13:139–50.
[55] Kildishev AV, Boltasseva A, Shalaev V. Planar photonics with metasurfaces. Science 2013;339:1232009.
[56] Yao AM, Padgett MJ. Orbital angular momentum: origins, behaviour and applications. Adv Opt Photon 2011;3:161–204.

[57] Franke-Arnold S, Radwell N. Light served with a twist. Opt Photon News 2017;28:28–35.
[58] Willner AE, Ren Y, Xie G, et al. Recent advances in high-capacity free-space optical and radio-frequency communications using orbital angular momentum multiplexing. Phil Trans R Soc A 2017;375:20150439.
[59] Wang J. Advances in communications using optical vortices. Photon Res 2016;4:B14–28.
[60] Manuel E, Fickler R, Krenn M, Zeilinger A. Twisted photons: new quantum perspective in high dimensions. Light Sci Appl 2018;7:17146.
[61] Ohtomo T, Chu SC, Otsuka K. Generation of vortex beams from lasers with controlled Hermite- and Ince-Gaussian modes. Opt Express 2008;16:5082–94.
[62] Chu SC, Chen YT, Tsai KF, Otsuka K. Generation of high-order Hermite-Gaussian modes in end-pumped solid state lasers for square vortex array laser beam generation. Opt Express 2012;20:7128–41.
[63] Kotlyar VV, Kovalev AA, Porfirev AP. Astigmatic laser beams with a large orbital angular momentum. Opt Express 2018;26:141–56.
[64] Heckenberg NR, McDuff R, Smith CP, White AG. Generation of optical phase singularities by computer-generated holograms. Opt Lett 1992;17:221–3.
[65] Biener G, Niv A, Kleniner V, Hasman E. Formation of helical beams by use of Pancharatnam-Berry phase optical elements. Opt Lett 2002;27:1875–7.
[66] Marrucci L, Manzo C, Paparo D. Optical spin-to-orbital angular momentum conversion in inhomogeneous anisotropic media. Phys Rev Lett 2006;96:1639051–4.
[67] Naidoo D, Roux FS, Dudley A, et al. Controlled generation of higher-order Poincaré sphere beams from a laser. Nat Photon 2016;10:327–32.
[68] Yi XN, Ling XH, Zhang ZY, et al. Generation of cylindrical vector vortex beams by two cascaded metasurfaces. Opt Express 2014;22:17207–15.
[69] Yue FY, Wen DD, Xin JT, Gerardot BD, Li JS, Chen XZ. Vector vortex beam generation with a single plasmonic metasurface. ACS Photonics 2016;3:1558–63.
[70] Liu YC, Ke YG, Zhou JX, et al. Generation of perfect vortex and vector beams based on Pancharatnam-Berry phase elements. Sci Rep 2017;7:44096.
[71] Zhang Y, Liu W, Gao J, Yang X. Generating focused 3D perfect vortex beams by plasmonic metasurfaces. Adv Opt Mater 2018;6:1701228.
[72] Ostrovsky AS, Rickenstorff-Parrao C, Arrizón V. Generation of the "perfect" optical vortex using a liquid-crystal spatial light modulator. Opt Lett 2013;38:534–6.
[73] Vaity P, Rusch L. Perfect vortex beam: Fourier transformation of a Bessel beam. Opt Lett 2015;40:597–600.
[74] Deng D, Li Y, Han YH, et al. Perfect vortex in three-dimensional multifocal array. Opt Express 2016;24:28270–8.
[75] Forbes A. Controlling light's helicity at the source: orbital angular momentum states from lasers. Phil Trans R Soc A 2017;375:20150436.
[76] Rubinsztein-Dunlop H, Forbes A, Berry MV, et al. Roadmap on structured light. J Opt 2016;19:013001.
[77] Alfano RR, Milione G, Galvez EJ, Shi L. Optical sources: a laser for complex spatial modes. Nat Photon 2016;10:286–8.
[78] Berry MV. Optical vortices evolving from helicoidal integer and fractional phase steps. J Opt A: Pure Appl Opt 2004;6:259.
[79] Seniutinas G, Balčytis A, Reklaitis I, et al. Tipping solutions: emergering 3D nano-fabrication/-imaging technologies. Nanophotonics 2017;6:923–41.
[80] Malinauskas M, Farsari M, Piskarskas A, Juodkzis S. Ultrafast laser nanostructruing of photopolymers: a decade of advances. Phys Rep 2013;533:1–31.
[81] Wang X, Kuchmizhak A, Storozhenko D, Makarov SV, Juodkazis S. Single-step laser plasmonic coloration of metal films. ACS Appl Mater Interfaces 2018;10:1422–7.
[82] Zhang YL, Chen QD, Xia H, Sun HB. Designable 3D nanofabrication by femtosecond laser direct writing. Nano Today 2010;5:435–48.
[83] Sugioka K. Progress in ultrafast laser processing and future prospects. Nanophotonics 2017;6:393–413.
[84] Wang L, Chen QD, Cao XW, et al. Plasmonic nano-printing: large-area nanoscale energy deposition for efficient surface texturing. Light Sci Appl 2017;6:e17112.
[85] Wang XW, Seniutinas G, Balcytis A, et al. Laser structuring for control of coupling between THz light and phonon modes. J Laser Micro Nanoen 2016;11:377–80.
[86] Brasselet E, Malinauskas M, Žukauskas A, Juodkazis S. Photopolymerized microscopic vortex beam generators: precise delivery of optical orbital angular momentum. Appl Phys Lett 2010;97:211108.
[87] Sun J, Wang X, Xu T, Kudyshev ZA, Cartwright AN, Lichinitser NM. Spinning light on the nanoscale. Nano Lett 2014;14:2726–9.
[88] Chong KE, Staude I, James A, et al. Polarization-independent silicon metadevices for efficient optical wavefront control. Nano Lett 2015;15:5369–74.
[89] Weber K, Hütt F, Thiele S, Gissibl T, Herkommer A, Giessen H. Single mode fiber based delivery of OAM light by 3D laser direct writing. Opt Express 2017;25:19672–79.
[90] Yu N, Genevet P, Kats MA, et al. Light propagation with phase discontinuities: generalized laws of reflection and refraction. Science 2011;334:333–7.
[91] Chen HT, Taylor AJ, Yu N. A review of metasurfaces: physics and appplications. Rep Prog Phys 2016;79:76401.
[92] Glybovski SB, Tretyakov SA, Belov PA, Kivshar YS, Simovski CR. Metasurfaces: from microwaves to visible. Phys Rep 2016;634:1–72.
[93] Ding F, Pors A, Bozhevolnyi SI. Gradient metasurfaces: a review of fundamentals and applications. Rep Prog Phys 2018;81:26401.
[94] Bharadwaj P, Deutsch B, Novotny L. Optical Antennas. Adv Opt Photon 2009;1:438–83.
[95] Novotny L, Hulst NV. Antennas for light. Nat Photon 2011;5:83–90.
[96] Arbabi A, Faraon A. Fundamental limits of ultrathin metasurfaces. Sci Rep 2017;7:43722.
[97] Kim M, Wong AMH, Eleftheriades GV. Optical Huygens' metasurfaces with independent control of the magnitude and phase of the local reflection coefficients. Phys Rev X 2014;4:41042.
[98] Monticone F, Estakhri NM, Alù A. Full control of nanoscale optical transmission with a composite metascreen. Phys Rev Lett 2013;110:203903.
[99] Decker M, Staude I, Falkner M, et al. High-efficiency dielectric Huygens' surface. Adv Opt Mater 2015;3:813–20.
[100] Zhao Q, Zhou J, Zhang F, Lippens D. Mie resonance-based dielectric metamaterials. Mater Today 2009;12:60–9.

[101] Zhou L, Withayachumnankul W, Shah CM, et al. Dielectric resonator nanoantennas at visible frequencies. Opt Express 2013;21:1344–52.
[102] Arbabi A, Horie Y, Ball AJ, Bagheri M, Faraon A. Subwavelength-thick lenses with high numerical apertures and large efficiency based on high-contrast transmit arrays. Nat Commun 2015;6:7069.
[103] Genevet P, Capasso F, Aieta F, Khorasaninejad M, Devlin R. Recent advances in planar optics: from plasmonic to dielectric metasrfaces. Optica 2017;4:139–52.
[104] Yu YF, Zhu AY, Paniagua-Domínguez R, Fu YH, Luk'yanchuk B, Kuznetsov AI. High-transmission dielectric metasurface with 2π phase control at visible wavelengths. Laser Photo Rev 2015;9:412–8.
[105] Shalaev MI, Sun J, Tsukernik A, Pandey A, Nikolskiy K, Litchinitser NM. High-efficiency all-dielectric metasurfaces for ultracompact beam manipulation in transmission mode. Nano Lett 2015;15:6261–6.
[106] Kuznetsov AI, Miroshnichenko AE, Brongersma ML, Kivshar Y, Luk'yanchuk B. Optically resonant dielectric nanostructures. Science 2016;354:AAG2472.
[107] Huang L, Chen X, Mühlenbernd H, et al. Three-dimensional optical holography using a plasmonic metasurface. Nat Commun 2013;4:2808.
[108] Genevet P, Capasso F. Holographic optical metasurfaces: a review of current progress. Rep Prog Phys 2015;78:24401.
[109] Ni X, Kildishev AV, Shalaev VM. Metasurface holograms for visible light. Nat Commun 2013;4:2807.
[110] Huang K, Liu H, Restuccia S, et al. Spiniform phase-encoded metagratings entangling arbitrary rational-order orbital angular momentum. Light Sci Appl 2018;7:17156.
[111] Zhan A, Colburn S, Trivedi R, Freyett TK, Dodson CM, Majumdar A. Low-contrast dielectric metasurface optics. ACS Photonics 2016;3:209–14.
[112] Min C, Liu J, Lei T, et al. Plasmonic nano-slits assisted polarization selective detour phase meta-hologram. Laser Photon Rev 2016;10:978–95.
[113] Wen D Yue F, Li G, et al. Helicity multiplexed broadband metasurface holograms. Nat Commun 2015;6:8241.
[114] Ye W, Zeuner F, Li X, et al. Spin and wavelength multiplexed nonlinear metasurface holography. Nat Commun 2016;7:11930.
[115] Li Y, Li X, Chen L, et al. Orbital angular momentum multiplexing and demultiplexing by a single metasurface. Adv Opt Mater 2017;5:1600502.
[116] Pancharatnam S. Generalized theory of interference and its applications: part I. coherent pencils. Proc India Acad Sci Sect A 1956;44:247–62.
[117] Berry MV. Quantal phase factors accompanying adiabatic changes. Proc R Soc London 1984;392:45–57.
[118] Berry MV. The adiabatic phase and Pancharatnam's phase for polarized light. J Mod Opt 1987;34:1401–7.
[119] Labrunie G, Robert J. Transient behaviour of the electrically controlled birefringence in a nematic liquid crystals. J Appl Phys 1973;44:4869.
[120] Yang L, Fan F, Chen M, Zhang X, Bai J, Chang S. Magnetically induced birefringence of randomly aligned liquid crystals in the terahertz regime under a weak magnetic field. Opt Mater Express 2016;6:2803–11.
[121] Primak W, Post D. Phtoelastic constants of vitreous silica and its elastic coefficient of refractive index. J Appl Phys 1959;30:779–88.
[122] Zhu Z, Brown TG. Stress-induced birefringence in microstructured optical fibers. Opt Lett 2003;28:2306–8.
[123] Grann EB, Moharam MG, Pommet DA. Artificial uniaxial and biaxial dielectrics with use of two-dimensional subwavelength binary gratings. J Opt Soc Am A 1994;11:2695–703.
[124] Elser J, Wangberg R, Podolskiy VA. Nanowire metamaterials with extreme optical anisotropy. Appl Phys Lett 2006;89:261102.
[125] Hao J, Yuan Y, Ran L, et al. Manipulating electromagnetic wave polarizations by anisotropic metamaterials. Phys Rev Lett 2007;99:63908.
[126] Thomhrattanasiri S, Podolskiy VA. Hypergratings: nanophotonics in planar anisotropic metamaterials. Opt Lett 2009;34:890–2.
[127] Hasman E, Kleiner V, Biener G, Niv A. Polarization dependent focusing lens by use of quantized Pancharatnam-Berry phase diffractive optics. Appl Phys Lett 2003;82:328.
[128] Lin D, Fan P, Hasman E, Brongersma ML. Dielectric gradient metasurface optical elements. Science 2014;345:298–302.
[129] Maguid E, Yulevich I, Veksler D, Kleiner V, Brongersma ML, Hasman E. Photonics spin-controlled multifunctional shared-aperture antenna array. Science 2016;352:1202–6.
[130] Bliokh KY. Geometrical optics of beams with vortices: Berry phase and orbital angular momentum Hall effect. Phys Rev Lett 2006;97:43901.
[131] Xiao S, Wang J, Liu F, Zhang S, Yin X, Li J. Spin-dependent optics with metasurfaces. Nanophotonics 2017;6:215–34.
[132] Ling X, Zhou X, Huang K, et al. Recent advances in the spin Hall effect of light. Rep Prog Phys 2017;80:664011–7.
[133] Cardano F, Marrucci L. Spin-orbit photonics. Nat Photon 2015;9:776–8.
[134] Bliokh KY, Rodríguez-Fortuño FJ, Zayats AV. Spin-orbit interactions of light. Nat Photon 2015;9:796–808.
[135] Shitrit N, Yulevich I, Maguid E, et al. Spin-optical metamaterial route to spin-controlled photonics. Science 2013;340:724–6.
[136] Chen H, Chen Z, Li Q, Lv H, Yu Q, Yi X. Generation of vector beams based on dielectric metasurfaces. J Mod Opt 2015;62:638–43.
[137] Karimi E, Schulz SA, Leon ID, Qassim H, Upham J, Boyd RW. Generating optical orbital angular momentum at visible wavelengths using a plasmonic metasurface. Light Sci Appl 2014;3:e167.
[138] Pu M, Li X, Ma X, et al. Cantenary optics for achromatic generation of perfecr optical angular momentum. Sci Adv 2015;1:E1500396.
[139] Hakobyan D, Magallanes H, Seniutinas G, Juodkazis S, Brasselet E. Tailoring orbital angular momentum of light in the visible domain with metallic metasurfaces. Adv Opt Mater 2016;4:306–12.
[140] Devlin RC, Ambrosio A, Wintz D, et al. Spin-to-orbital angular momentum conversion in dielectric metasurfaces. Opt Express 2017;25:377–93.
[141] Wang X, Kuchmizhak AA, Brasselet E, Juodkazis S. Dielectric geometric phase optical elements fabricated by femtosecond direct laser writing in photoresists. Appl Phys Lett 2017;110:1–4.
[142] Yang Y, Wang W, Moitra P, Kravchenko II, Briggs DP, Valentine J. Dielectric meta-reflectarray for broadband linear polarization conversion and optical vortex generation. Nano Lett 2014;14:1394–9.

[143] Huang L, Chen X, Mühlenbernd H, et al. Dispersionless phase discontinuities for controlling light propagation. Nano Lett 212;12:5750–5.
[144] Wang S, Wu PC, Su VC, et al. Broadband achromatic optical metasurface devices. Nat Commun 2017;8:187.
[145] Wang S, Wu PC, Su VC, et al. A broadband achromatic metalens in the visible. Nat Nanotechnol 2018;13:227–32.
[146] Chen WT, Zhu AY, Sanjeev V, et al. A broadband achromatic metalens for focusing and imaging in the visible. Nat Nanotechnol 2018;13:220–6.
[147] Shi Z, Khorasaninejad M, Huang YW, et al. Single-layer metasurface with controlloable multiwavelength functions. Nano Lett 2018;18:2420–7.
[148] Arbabi A, Horie Y, Bagheri M, Faraon A. Dielectric metasurfaces for complete control of phase and polarization with subwavelength spatial resolution and high transmission. Nat Nanotechnol 2015;10:937–44.
[149] Zhou J, Liu Y, Ke Y, Luo H, Wen S. Generation of Airy vortex and Airy vector beams based on the modulation of dynamic and geometric phase. Opt Lett 2015;40:3193–6.
[150] Chen S, Cai Y, Li G, Zhang S, Cheah KW. Geometric metasurface fork gratings for vortex-beam generation and manipulation. Laser Photon Rev 2016;10:322–6.
[151] Fan Q, Wang D, Huo P, Zhang Z, Liang Y, Xu T. Autofocusing Airy beams generated by all-dielectric metasurface for visible light. Opt Express 2017;25:9285–94.
[152] Zhang L, Liu S, Li L, Cui TJ. Spin-controlled multiple pencil beams and vortex beams with different polarizations generated by Pancharatnam-Berry coding metasurfaces. ACS Appl Mater Interfaces 2017;9:36447–55.
[153] Yue F, Wen D, Zhang C, et al. Multichannel polarization controllable superpositions of orbital angular momentum states. Adv Mater 2017;29:1603838.
[154] Ling X, Zhou X, Yi X, et al. Giant photonics spin Hall effect in momentum space in a structured metamaterial with spatially varying birefringence. Light Sci Appl 2015;4:e290.
[155] Niv A, Gordodetski Y, Kleiner V, Hasman E. Topological spin-orbit interaction of light in anisotropic inhomogeneous subwavelength structures. Opt Lett 2008;33:2910–2.
[156] Devlin RC, Ambrosio A, Rubin NA, Mueller JPB, Capasso F. Arbitrary spin-to-orbital angular momentum conversion of light. Science 2017;358:896–901.
[157] Wang X, Kuchmizhak A, Hu D, Li X. Multiple orbital angular momentum generated by dielectric hybrid phase element. AIP Conf Proc 2017;1874:30039.
[158] Mueller JPB, Rubin NA, Devlin RC, Groever B, Capasso F. Metasurface polarization optics: independent phase control of arbitrary orthogonal states of polarization. Phys Rev Lett 2017;118:113901.
[159] Ma Q, Shi CB, Bai GD, Chen TY, Noor A, Cui TJ. Beam-editing coding metasurfaces based on polarization bit and orbital angular momentum mode bit. Adv Opt Mater 2017;5:1700548.
[160] Oron R, Davidson N, Friesem AA, Hasman E. Efficient formation of pure helical laser beams. Opt Commun 2000;182:205–8.
[161] Ngcobo S, Litvin IA, Burger L, Forbes A. A digital laser for on-demand laser modes. Nat Commun 2013;4:2289.
[162] Lin D, Daniel J, Clarkson W. Controlling the handedness of directly excited Laguerre–Gaussian modes in a solid-state laser. Opt Lett 2014;39:3903–6.
[163] Kim D, Kim J. Direct generation of an optical vortex beam in a single-frequency Nd: YVO 4 laser. Opt Lett 2015;40:399–402.
[164] Leger JR, Chen D, Dai K. High modal discrimination in a Nd: YAG laser resonator with internal phase gratings. Opt Lett 1994;19:1976–8.
[165] Caley AJ, Thomson MJ, Liu J, Waddie AJ, Taghizadeh MR. Diffractive optical elements for high gain lasers with arbitrary output beam profiles. Opt Express 2007;15:10699–704.
[166] Naidoo D, Aït-Ameur K, Brunel M, Forbes A. Intra-cavity generation of superpositions of Laguerre–Gaussian beams. Appl Phys B 2012;106:683–90.
[167] Litvin IA, Burger L, Forbes A. Petal-like modes in Porro prism resonators. Opt Express 2007;15:14065–77.
[168] Bourderionnet J, Brignon A, Huignard JP, Delboulbe A, Loiseaux B. Spatial mode control of a diode-pumped Nd: YAG laser by an intracavity liquid-crystal light valve. Opt Lett 2001;26:1958–60.
[169] Ito A, Kozawa Y, Sato S. Generation of hollow scalar and vector beams using a spot-defect mirror. JOSA A 2010;27:2072–7.
[170] Thirugnanasambandam M, Senatsky Y, Ueda K. Generation of very – high order Laguerre-Gaussian modes in Yb: YAG ceramic laser. Laser Phys Lett 2010;7:637–43.
[171] Bisson J, Senatsky Y, Ueda K. Generation of Laguerre-Gaussian modes in Nd: YAG laser using diffractive optical pumping. Laser Phys Lett 2005;2:327–33.
[172] Tovar AA. Production and propogation of cylindrically polarized Laguerre-Gaussian laser beams. JOSA 1998;15:2705–11.
[173] Zhan Q. Cylindrical vector beams: from mathematical concepts to applications. Adv Opt Photon 2009;1:1–57.
[174] Chen J, Wan C, Zhan Q. Vectorial optical fields: recent advances and future prospects. Sci Bull 2018;63:54–74.
[175] Milione G, Sztul H, Nolan D, Alfano R. Higher-order Poincaré sphere, Stokes parameters, and the angular momentum of light. Phys Rev Lett 2011;107:053601.
[176] Padgett MJ, Courtial J. Poincaré-sphere equivalent for light beams containing orbital angular momentum. Optics Lett 1999;24:430–2.
[177] Marrucci L, Karimi E, lussarenko S, et al. Spin-to-orbital conversion of the angular momentum of light and its classical and quantum applications. J Opt 2011;13:064001.
[178] Zhao Y, Edgar JS, Jeffries GD, McGloin D, Chiu DT. Spin-to-orbital angular momentum conversion in a strongly focused optical beam. Phys Rev Lett 2007;99:073901.
[179] Liang Y, Wu HW, Huang BJ, Huang XG. Light beams with selective angular momentum generated by hybrid plasmonic waveguides. Nanoscale 2014;6:12360–5.
[180] Liang Y, Zhang F, Gu J, Huang XG, Liu S. Integratable quarter-wave plates enable one-way angular momentum conversion. Sci Rep 2016;6:24959.
[181] Liang Y, Huang X. Generation of two beams of light carrying spin and orbital angular momenta of opposite handedness, Opt Lett 2014;39:5074–7.
[182] Zhang F, Liang Y, Zhang H, et al. Optical gears in a nanophotonic directional coupler. Opt Express 2017;25:10972–83.
[183] Kim D, Kim J, Clarkson W. Q-switched Nd: YAG optical vortex lasers. Opt Express 2013;21:29449–54.
[184] Zhang Y, Yu H, Zhang H, Xu X, Xu J, Wang J. Self-mode-locked Laguerre-Gaussian beam with staged topological charge by thermal-optical field coupling. Opt Express 2016;24:5514–22.

[185] Li H, Phillips DB, Wang X, et al. Orbital angular momentum vertical-cavity surface-emitting lasers. Optica 2015;2:547–52.
[186] Cai X, Wang J, Strain MJ, et al. Integrated compact optical vortex beam emitters. Science 2012;338:363–6.
[187] Xie Z, Lei T, Li F, et al. Ultra-broadband on-chip twisted light emitter for optical communications. Light Sci Appl 2018;7:18001.
[188] Maltese G, Halioua Y, Lemaître A, et al. Towards an integrated AlGaAs waveguide platform for phase and polarisation shaping. J Opt 2018;20:05LT01.
[189] Miao P, Zhang Z, Sun J, et al. Orbital angular momentum microlaser. Science 2016;353:464–7.
[190] Guo J, Liang Y, Huang XG, Guo B, Li J. Pure dielectric waveguides enable compact, ultrabroadband wave plates. IEEE Photonics J 2016;8:1–9.
[191] Zhang F, Liang Y, Zhang H, et al. On chip chirality-distinguishing beamsplitter. Opt Express 2017;25:24861–71.
[192] Chong A, Buckley J, Renninger W, Wise F. All-normal-dispersion femtosecond fiber laser. Opt Express 2006;14:10095–100.
[193] Jeong Y, Sahu J, Payne D, Nilsson J. Ytterbium-doped large-core fiber laser with 1.36 kW continuous-wave output power. Opt Express 2004;12:6088–92.
[194] Lira H, Yu Z, Fan S, Lipson M. Electrically driven nonreciprocity induced by interband photonic transition on a silicon chip. Phys Rev Lett 2012;109:033901.
[195] Yu Z, Veronis G, Wang Z, Fan S. One-way electromagnetic waveguide formed at the interface between a plasmonic metal under a static magnetic field and a photonic crystal. Phys Rev Lett 2008;100:023902.
[196] Rüter CE, Makris KG, El-Ganainy R, Christodoulides DN, Segev M, Kip D. Observation of parity–time symmetry in optics. Nat Phys 2010;6:192–5.
[197] Feng L, El-Ganainy R, Ge L. Non-Hermitian photonics based on parity–time symmetry. Nat Photon 2017;11:752–62.
[198] Leach J, Yao E, Padgett MJ. Observation of the vortex structure of a non-integer vortex beam. New J Phys 2004;6:71.
[199] Oemrawsingh SSR, Ma X, Voigt D, et al. Experimental demonstration of fractional orbital angular momentum entanglement of two photons. Phys Rev Lett 2005;95:240501.
[200] Yang Z, Zhang X, Bai C. Nondiffracting light beams carrying fractional orbital angular momentum. JOSA A 2018;35:452–61.
[201] Basistiy IV, Pas'Ko VA, Slyusar VV, Soskin MS, Vasnetsov MV. Synthesis and analysis of optical vortices with fractional topological charges. J Opt A: Pure Appl Opt 2004;6:S166.
[202] Tao SH, Yuan XC, Lin J, Peng X, Niu HB. Fractional optical vortex beam induced rotation of particles. Opt Express 2005;13:7726–31.
[203] Götte JB, Franke-Arnold S, Zambrini R, Barnett SM. Quantum formulation of fractional orbital angular momentum. J Mod Opt 2007;54:1723–38.
[204] Götte JB, O'Holleran K, Preece D, et al. Light beams with fractional orbital angular momentum and their vortex structure. Opt Express 2008;16:993–1006.
[205] O'Dwyer DP, Phelan CF, Rakovich YP, Eastham PR, Lunney JG, Donegan JF. Generation of continuously tunable fractional optical orbital angular momentum using internal conical diffraction. Opt Express 2010;18:16480–5.
[206] Turpin A, Rego L, Picón A, Román JS, Hernández-García C. Extreme ultraviolet fractional orbital angular momentum beams from high harmonic generation. Sci Rep 2017;7:43888.
[207] Wang Y, Zhao P, Feng X, et al. Dynamically sculpturing plasmonic vortices: from integer to fractional orbital angular momentum. Sci Rep 2016;6:36269.
[208] Martinez-Castellanos I, Gutiérrez-Vega JC. Shaping optical beams with non-integer orbital-angular momentum: a generalized differential operator approach. Opt Lett 2015;40:1764–7.
[209] Berkhout GCG, Lavery MPJ, Padgett MJ, Beijersbergen MW. Measuring orbital angular momentum superpositions of light by mode transformation. Optics Lett 2011;36:1863–5.
[210] Fickler R, Lapkiewicz R, Huber M, Lavery MPJ, Padgett MJ, Zeilinger A. Interface between path and orbital angular momentum entanglement for high-dimensional photonic quantum information. Nat Commun 2014;5:4502.
[211] Zhou J, Zhang WH, Chen LX. Experimental detection of high-order or fractional orbital angular momentum of light based on a robust mode converter. Appl Phys Lett 2016;108:111108.
[212] Abramochkin EG, Volostnikov VG. Generalized Gaussian beams. J Opt A: Pure Appl Opt 2004;6:S157.
[213] Tung JC, Omatsu T, Liang HC, Huang KF, Chen YF. Exploring the self-mode locking and vortex structures of nonplanar elliptical modes in selectively end-pumped Nd: YVO 4 lasers: manifestation of large fractional orbital angular momentum. Opt Express 2017;25:22769–79.
[214] Vyas S, Senthilkumaran P. Interferometric optical vortex array generator. Appl Opt 2007;46:2893–8.
[215] Ladavac K, Grier DG. Microoptomechanical pumps assembled and driven by holographic optical vortex arrays. Opt Express 2004;12:1144–9.
[216] Becker J, Rose P, Boguslawski M, Denz C. Systematic approach to complex periodic vortex and helix lattices. Opt Express 2011;19:9848–62.
[217] Zhang N, Yuan XC, Burge RE. Extending the detection range of optical vortices by Dammann vortex gratings. Opt Lett 2010;35:3495–7.
[218] Lei T, Zhang M, Li YR, et al. Massive individual orbital angular momentum channels for multiplexing enabled by Dammann gratings. Light Sci Appl 2015;4:e257.
[219] Berkhout GCG, Lavery MPJ, Courtial J, Beijersbergen MW, Padgett MJ. Efficient sorting of orbital angular momentum states of light. Phys Rev Lett 2010;105:153601.
[220] Mirhosseini M, Malik M, Shi Z, Boyd RW. Efficient separation of the orbital angular momentum eigenstates of light. Nat Commun 2013;4:2781.
[221] Ren HR, Li XP, Zhang QM, Gu M. On-chip noninterference angular momentum multiplexing of broadband light. Science 2016;352:805–9.
[222] Yan Y, Xie GD, Lavery MPJ, et al. High-capacity millimetre-wave communications with orbital angular momentum multiplexing. Nat Commun 2014;5:4876.
[223] Yan Y, Yue Y, Huang H, et al. Multicasting in a spatial division multiplexing system based on optical orbital angular momentum. Opt Lett 2013;38:3930–3.
[224] Zhu L, Wang J. Simultaneous generation of multiple orbital angular momentum (OAM) modes using a single phase-only element. Opt Express 2015;23:26221–33.
[225] Du J, Wang J. Design of on-chip N-fold orbital angular momentum multicasting using V-shaped antenna array. Sci Rep 2015;5:9662.

[226] Pozar DM, Targonski SD. A shared-aperture dual-band dual-polarized microstrip array. IEEE Trans Antennas Propag 2001;49:150–7.
[227] Lager IE, Trampuz C, Simeoni M, Ligthart LP. Interleaved array antennas for FMCW radar applications. IEEE Trans Antennas Propag 2009;57:2486–90.
[228] Maguid E, Yulevich, I, Yannai M, Kleiner V, Brongersma ML, Hasman E. Multifunctional interleaved geometric-phase dielectric metasurfaces. Light Sci Appl 2017;6:e17027.
[229] Li S, Wang J. Adaptive power-controllable orbital angular momentum (OAM) multicasting. Sci Rep 2015;5:9677.
[230] Zhu L, Wang J. Arbitrary manipulation of spatial amplitude and phase using phase-only spatial light modulators. Sci Rep 2014;4:7441.
[231] Li S, Wang J. Compensation of a distorted N-fold orbital angular momentum multicasting link using adaptive optics. Opt Lett 2016;41:1482–5.
[232] Zhu L, Wang J. Demonstration of obstruction-free data-carrying N-fold Bessel modes multicasting from a single Gaussian mode. Opt Lett 2015;40:5463–6.
[233] Zhao Y, Xu J, Wang A, et al. Demonstration of data-carrying orbital angular momentum-based underwater wireless optical multicasting link. Opt Express 2017;25:28743–51.
[234] Lin YC, Lu TH, Huang KF, Chen YF. Generation of optical vortex array with transformation of standing-wave Laguerre-Gaussian mode. Opt Express 2011;19:10293–303.
[235] Son B, Kim S, Kim YH, et al. Optical vortex arrays from sematic liquid crystals. Opt Express 2014;22:4699–704.
[236] Du J, Wang J. Chip-scale optical vortex lattice generator on silicon platform. Opt Lett 2017;42:5054–7.
[237] Huang LL, Song X, Reineke B, et al. Volumetric generation of optical vortices with metasurfaces. ACS Photon 2017;4:338–6.
[238] Mehmood MQ, Mei ST, Hussain S, et al. Visible-frequency metasurface for Structuring and spatially multiplexing Optical Vortices. Adv Mater 2016;28:2533–9.
[239] Yue FY, Wen DD, Zhang C, et al. Multichannel polarization-controllable superpositions of orbital angular momentum states. Adv Mater 2017;29:1603838.
[240] Jin JJ, Pu MB, Wang YQ, et al. Multi-channel vortex beam generation by simultaneous amplitude and phase modulation with two-dimensional metamaterial. Adv Mater Technol 2017;2:1600201.
[241] Gao H, Li Y, Chen LW, et al. Quasi-Talbot effect of orbital angular momentum beams for generation of optical vortex arrays by multiplexing metasurface design. Nanoscale 2018;10:666–71.